Meffin, H., B. Tahayori, E. N. Sergeev, I. M. Y. Mareels, D. B. Grayden and A. N. Burkitt (2014). Modelling extracellular electrical stimulation: part 3. Derivation and interpretation of neural tissue equations. Journal of Neural Engineering **11**(6): 065004.

DOI: 10.1088/1741-2560/11/6/065004

Modeling Extracellular Electrical Stimulation: III. Derivation and Interpretation of Neural Tissue Equations

Hamish Meffin[1,2], Bahman Tahayori[1], Evgeni N. Sergeev[1], Iven M.Y. Mareels[3], David B. Grayden[1,2,4], and Anthony N. Burkitt[1,2,4]

[1]NeuroEngineering Laboratory, Department of Electrical and Electronic Engineering, The University of Melbourne, VIC 3010, Australia

[2]NICTA Victoria Research Laboratory, Parkville, VIC 3010, Australia

[3]Melbourne School of Engineering, The University of Melbourne, VIC 3010, Australia

[4]Bionics Institute, East Melbourne, VIC 3002, Australia

E-mail: `hmeffin@unimelb.edu.au, bahmant@unimelb.edu.au`

Abstract. *Objective:* A common approach in modelling extracellular electrical stimulation is to represent neural tissue by a volume conductor when calculating the activating function as the driving term in a cable equation for the membrane potential. This approach ignores the cellular composition of tissue, including the neurites and their combined effect on the extracellular potential. This has a number of undesirable consequences. First, the two natural and equally valid choices of boundary conditions for the cable equation (i.e. using either voltage or current) lead to two mutually inconsistent predictions of the membrane potential. Second, the spatio-temporal distribution of the extracellular potential can be strongly affected by the combined cellular composition of the tissue. In this paper, we develop a mean field volume conductor theory to overcome these shortcomings of available models. *Approach:* This method connects the microscopic properties of the constituent fibres to the macroscopic electrical properties of the tissue by introducing an admittivity kernel for the neural tissue that is non-local, non-instantaneous and anisotropic. This generalises the usual tissue conductivity. A class of bidomain models that is mathematically equivalent to this class of self-consistent volume conductor models is also presented. The bidomain models are computationally convenient for simulating the activation map of neural tissue using numerical methods such as finite element analysis. *Main results:* The theory is first developed for tissue composed of identical, parallel fibres and then extended to general neural tissues composed of mixtures of neurites with different and arbitrary orientations, arrangements and properties. Equations describing the extracellular and membrane potential for the longitudinal and transverse modes of stimulation are derived. *Significance:* The theory complements our earlier work, which developed extensions to cable theory for the micro-scale equations of neural stimulation that apply to individual fibres. The modeling framework provides a number of advantages over other approaches currently adopted in the literature and, therefore, can be used to accurately estimate the membrane potential generated by extracellular electrical stimulation.

1. Introduction

1.1. Background and Motivation

Extracellular neural stimulation is used in a wide variety of neuroprosthetic devices to restore lost neural function or treat medical conditions. Examples include cardiac pacemakers, cochlear implants, some prosthetic limbs, bionic eyes and deep brain stimulators for the treatment of Parkinson's disease or epilepsy (e.g. [1–10]). Novel strategies for electrical stimulation have improved outcomes for patients, for example by using new stimulus waveforms or by employing novel temporal or spatial patterns of stimulus pulses. However, the effect of spatial and temporal interactions between electrodes on neural activity can be difficult to predict without the use of accurate models. As a result, electrical stimulation of excitable cells has attracted considerable attention during the past few decades from modelers as well as theorists [11–19].

In this paper, we consider from a theoretical perspective, how the cellular composition of tissue affects extracellular electrical stimulation. Neural tissue is composed of tightly packed cells, neurons and glia, forming a matrix that is highly heterogeneous on a microscopic scale (see Figure 2(a)). Membranes partition the extracellular space from the intracellular space, and each of these components (membranes, extracellular space and intracellular space) have distinct electrical properties. The electrical impedance of cellular membranes is high compared to that of the extra- or intra-cellular space. It also contains capacitive as well as resistive components, in contrast to the extra- and intra-cellular space, which are purely resistive. The extracellular space is extremely confined, with a width in the range of 20-70nm (see [20–23]), which leads to a high effective resistivity for current passing through this space (for a vivid visualisation of this see [24] and the associated video). By contrast, the intracellular space is comparatively wide, with neurite diameters ranging from 0.5 μm for axons to many micrometers for dendrites. This results in comparatively low effective resistance in the direction along the neurite, allowing relatively easy passage of current in this direction, but only once the current has passed across the high impedance membrane.

Classic approaches to modelling extracellular electrical stimulation of tissue have largely ignored the effect of these microscale inhomogeneities. Two of the main modelling approaches are 1) a volume conductor approach and 2) a bidomain approach. Implicity or explicitly these approaches have assumed that these inhomogeneities can be locally averaged over space to give a spatially smooth description without significantly affecting the overall flow of current or the distribution of potential in the tissue. However, a derivation of these equations that explicitly involves spatial averaging has never been carried out, to the best of our knowledge. Here, we present such a detailed spatial averaging analysis that takes into account the locally heterogenous composition of tissue, including cellular geometry. The results lead to new forms for the standard equations for extracellular electrical stimulation of tissue, and suggest that the local heterogeneous microstructure of tissue significantly affects the global distribution of

potential and current density within the tissue. We begin by summarising the two classic modelling approaches; we review the strengths and weakness of each as background and motivation to the modelling framework presented here. Then we present a framework that unifies and builds upon these two approaches, and which takes into account the cellular composition of tissue.

1.2. Volume Conductor Models

Volume conductor-type models most frequently employ a two-stage approach [25]. Stage 1 involves the volume conductor model itself, which is a macroscopic description of the extracellular electrical potential and current flow through tissue from a set of electrodes. A defining feature is that the electrical properties of the tissue are described by its bulk conductivity, which is assumed to be smooth and homogeneous on a microscale. A Laplace-type equation governs the extracellular potential, which is the result of combining Ohm's Law and Kirchoff's Law in the form of partial differential equations [26]. Stage 2 calculates the membrane potential of a neurite at the microscopic scale. This is done by calculating either the extracellular potential or the extracellular current density on the outer surface of the neurite, as calculated from Stage 1, and then applying it to an equation to determine the membrane potential of the cell. Most typically, this is a cable equation, which describes activation of the cell via a longitudinal mode [11], in which current passes into the neurite and then along it as illustrated in Figure 1(a). Alternatively, activation could be via a transverse mode, in which current passes across the neurite, and which is described by an ordinary differential equation in time [25, 27]; the first two modes of transverse stimulation are shown in Figures 1(b) and 1(c).

This approach is reasonably straight-forward and is computationally efficient because it breaks the macroscopic and microscopic scales of the problem across the two stages, thus avoiding the need to perform a microscopic scale discretisation of the problem across a macroscopic spatial extent. However, it ignores the effect of the neurite itself on the extracellular potential, for the simple reason that the volume conductor model does not contain any model of the neurite [28]. While this effect has sometimes been assumed to be of minor importance, we recently showed that it can lead to large internal inconsistencies [29]: widely discrepant answers for the membrane potential result depending on whether current density or voltage is extracted from the Stage 1 volume conductor model to apply to the neurite equations in Stage 2. Furthermore, qualitatively different answers can arise between the two types of boundary conditions, whereby neural activation is predicted to occur via the longitudinal mode in one case and the transverse mode in the other.

Intuitively, this discrepancy arises because the two stages of the model are not consistent with each other. This can be understood in terms of the electrical transimpedance of the neurite, which characterises the relationship between electrical potential and the current density on its surface. The neurite in Stage 2 has its

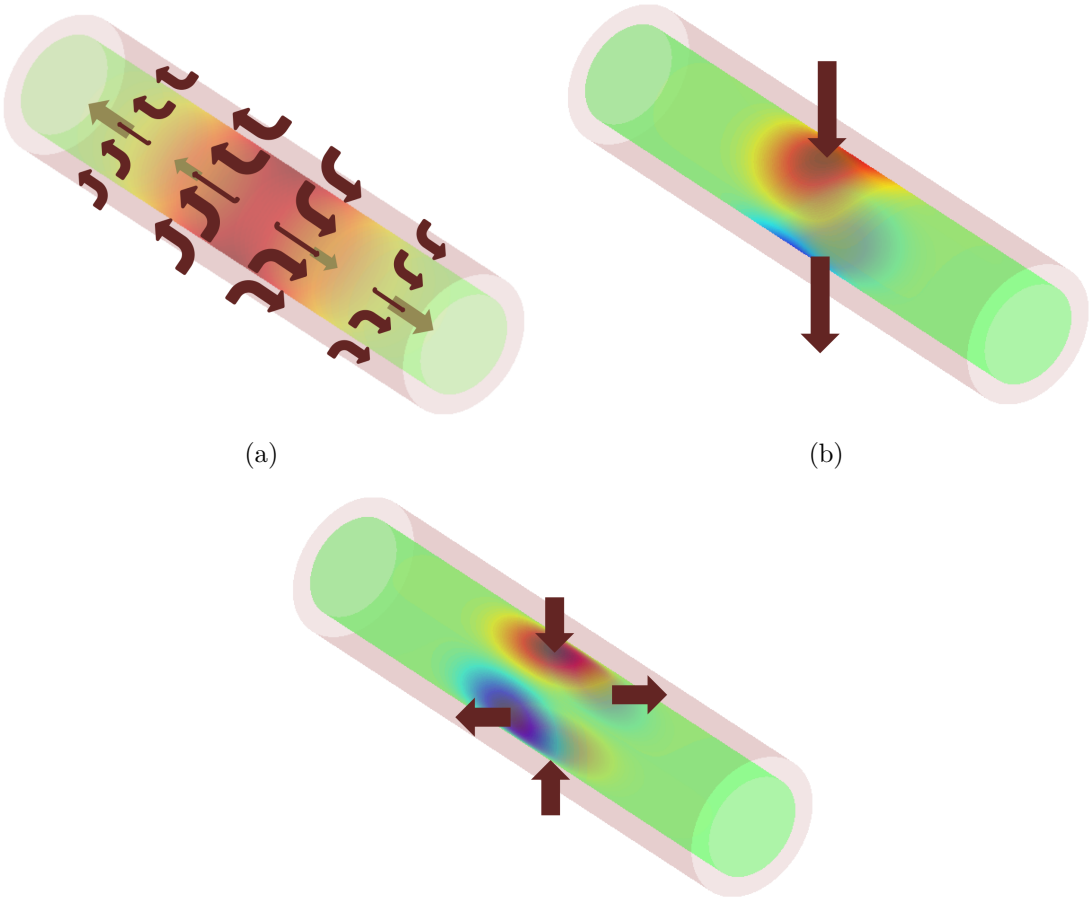

Figure 1. Visualisation of different components of stimulation characterised by an integer, n. (a) $n = 0$ represents the case where current flows internally along the neurite and is referred to as the longitudinal mode, (b) $n = 1$ is the first component of the transverse mode of stimulation where one side of the neurite is depolarised (red online) while the other side is hyperpolarised (blue online) relative to rest (green online), (c) for $n = 2$ two parts of the neurite are depolarised and two parts are hyperpolarised. See Table 1 for the mathematical description of n

own electrical transimpedance, which is typically different to the transimpedance of a corresponding volume in the volume conductor model. The mismatch between the Stage 1 and Stage 2 transimpedances gives rise to the inconsistency (i.e. answers that depend on the boundary condition type). A Stage 1 volume conductor model with electrical impedance that was derived from the transimpedance of the tissue's cellular constituents would resolve this inconsistency and more accurately model the tissue's electrical properties. ‡

‡ Potentially, this inconsistency can be overcome by placing a model of a single neurite in the volume conductor and calculating the extracellular potential, current density and membrane potential using this single model. By definition, this leads to a membrane potential that is independent of the type of boundary condition applied (i.e. consistent). However, because this model contains both microscopic

1.3. Bidomain Models

Bidomain models were originally developed to model cardiac tissue, but have since been extended to model neural tissue in the central nervous system. By contrast to volume conductors, bidomain models naturally avoid internal inconsistencies because all quantities are calculated in a single-step model. Bidomain models use two electrical continua (essentially two volume conductors): one to represent the extracellular space and another to represent the intracellular space. These domains are coupled together by the flow of current through a spatially continuous membrane [32,33]. A key point of this approach is that the extracellular, intracellular and membrane continua are all present at every point in space. Thus, the cellular geometry of the neurons and surrounding tissue is not modelled. This allows bidomain models to be computationally efficient. However, it has also been a weakness of bidomain models, as their ability to capture effects related to the microstructure of tissue and cellular geometry has been unclear (e.g., the ability to model the approximately-cylindrical shape of neurites).

In [34], a variant of the bidomain approach, referred to as the 'whole finite element' approach, is introduced. This three-dimensional model takes into account the morphology of the neurites under stimulation and uses a thin-film approximation to link the intracellular and extracellular boundary conditions.

1.4. Aims of the Paper

In this paper, we present a class of two-stage volume conductor models that accounts for the cellular composition of neural tissue. Essentially, this is achieved by matching the electrical transimpedance of a neurite to that of an equivalent volume in the volume conductor model. Critically, the approach can capture the effects of the cellular composition of tissue because the electrical transimpedance has the remarkable property of capturing not just the surface electrical properties of the neurite, but also its full internal electrical properties, including three-dimensional geometry [35]. The approach leads to a mathematical description of the tissue admittivity based on the properties of its cellular constituents. The admittivity replaces the conductivity of standard volume conductors. It is a complex number that quantifies the conductance and admittance of tissue, and is the reciprocal of impeditivity, which accounts for the resistive and capacitive properties of tissue. The resulting novel cellular composite volume conductor equations predict significant macro-scale effects on the magnitude and distribution of electrical potential and current density that are not accounted for in standard volume

and macroscopic scales, this approach requires either using highly simplified models that allow analytical calculation (such as a homogeneous volume conductor [13]) or resorting to numerical methods that become highly computationally challenging. Furthermore, such approaches do not account for the effect of neighbouring neurites, which have been shown to be significant in a number of recent studies [30,31], a finding that is corroborated in this study. Consequently, a volume conductor modelling framework that is self-consistent, computationally efficient and properly accounts for the cellular composition of tissue is lacking.

conductor frameworks. Furthermore, the framework is self-consistent, in the sense that the membrane potential is independent of the boundary condition type used in Stage 2.

We also present a class of bidomain models (or more generally multidomain models) that is mathematically equivalent to the class of cellular composite volume conductor models. This link to the cellular composite volume conductor models means that the bidomain models are also consistent with the electrical transimpedance of an individual neurite. Because the electrical transimpedance has the property, mentioned above, of capturing the full internal electrical properties of a neurite, including its three dimensional geometry [35], this provides a greater justification for the bidomain model by more clearly linking it to the underlying cellular geometry. Both types of model avoid the need to perform discretisation at fine spatial scales, and therefore are computationally tractable in general.

The modelling framework presented here completes our previously presented framework for Stage 2 of a volume conductor model [25]: it adds a self-consistent Stage 1 as well as an equivalent and alternative bidomain model. In this previous work, we derived the ordinary and partial differential equations governing the (linear) subthreshold membrane potential of a cylindrical neurite, given either extracellular current density or extracellular voltage boundary conditions on the surface of the cylinder. The derivation was performed from a full three-dimensional model of a cylindrical neurite plus thin extracellular sheath (NTES), as shown in Figure 2(e). The NTES is a key concept in this paper. The thin extracellular sheath models the extremely confined extracellular space ($\approx$ 60nm) that is typical of neural tissue [23], and which severely restricts extracellular current flow [36]. This is an important issue for modelling tissue admittivity as current flow through the extracellular space encounters much higher resistance than through the large intracellular space. The derivation from the three-dimensional model showed that, for the longitudinal mode of stimulation, two alternative cable equations for the membrane potential were recovered: one for voltage boundary conditions and another for current density boundary conditions (see Table 3 for the two equations). Interestingly, the electrotonic length constants differed between the two cases. For the transverse mode, an ordinary differential equation in time was derived for each boundary condition-type, in this case with different time constants (see Table 3). We also showed that this Stage 2 model gave membrane potential results that were consistent across boundary condition type (and resolved these apparent discrepancies in length and time constants) if and only if a set of transimpedance equations were obeyed that relate the extracellular current density on the boundary of the NTES to the extracellular potential (see Table 3).

Here, we show how to use this result to construct a Stage 1 volume conductor model that accounts for the cellular composition of tissue and gives self-consistent results when combined with the Stage 2 neurite equations for the membrane potential. This is done by using the NTES element as a building block, so that the cellular structure of tissue is treated as a composite of NTES elements in a mean-field approximation. This allows the derivation of the tissue admittivity from first principles. The new form of tissue

admittivity can affect the spatio-temporal pattern of current flow and potential in the tissue in ways that are not captured by standard volume conductor theory.

1.5. Organisation of the Paper

The paper is organised as follows. We initially focus on a simplified but biologically important tissue type, namely a fibre bundle consisting of identical parallel fibres. In Section 2.1, we define the underlying fundamental model of such a fibre bundle from which the approximately equivalent volume conductor and bidomain models will be derived. The mean-field derivation of the cellular composite volume conductor model for a fibre bundle follows in Section 2.2. The Analytical Results section begins by giving the full set of derived equations for the cellular composite volume conductor model for a fibre bundle (Section 3.1). The mathematically equivalent bidomain model is described in Section 3.2, with the proof of its equivalence given in Appendix D. The following section uses a mean-field approach to generalise the volume conductor and bidomain equations to the general case of tissue composed of neurites of an arbitrary variety of orientations and heterogeneous neurite types and cellular properties. Some associated derivations are given in Appendix D. The physical interpretation of the equations and their relation to other volume conductor or bidomain equations is discussed in Section 4.

2. Methods

The Methods section outlines the derivation of the cellular composite volume conductor model in the case of a bundle of identical parallel fibres. Generalisations of this and equivalent bidomain/multidomain models are derived in other sections of the paper as described immediately above.

2.1. Fundamental Model of a Fibre Bundle

Figure 2(a) shows a scanning electron micrograph of a nerve fibre bundle. The fundamental model of a fibre bundle used here is composed of closely packed, parallel fibres each of approximately the same dimensions. Let each fibre be orientated with its axis in the z-direction, have approximate cross-sectional width $2a$ and a separation from neighbouring fibres of approximately $2d$, as shown in Figure 2.

Laplace's equation [37] governs the spatial distribution of the intra- and extracellular potentials, $\phi_{\rm i}$ and $\phi_{\rm e}$, respectively: $\boldsymbol{\nabla}^2\phi_c = 0, \quad c = {\rm i, e}$. More fundamentally, the potentials are derived from a pair of equations consisting of a continuity equation for the current densities, $\boldsymbol{\Gamma}_{\rm i}$ and $\boldsymbol{\Gamma}_{\rm e}$, and a constitutive equation relating the current density to the potential,

$$\boldsymbol{\nabla}\cdot\boldsymbol{\Gamma}_c(x,y,z,t) = 0, \tag{1a}$$

$$\boldsymbol{\Gamma}_c(x,y,z,t) \quad = -\rho_c^{-1}\boldsymbol{\nabla}\phi_c(x,y,z,t), \tag{1b}$$

where (x, y, z) is any point in the intracellular space if $c = \mathrm{i}$, or in the extracellular space if $c = \mathrm{e}$. ρ_i and ρ_e are the intracellular and extracellular resistivities, respectively.

The boundary conditions ensure continuity of current across the neural membrane and boundedness of the potential for all space and time:

$$\frac{1}{\rho_\mathrm{i}}\frac{\partial\phi_\mathrm{i}(x,y,z,t)}{\partial n} = -J_\mathrm{m}(x,y,z,t), \quad \forall(x,y,z) \in \text{any membrane}, \tag{2a}$$

$$\frac{1}{\rho_\mathrm{e}}\frac{\partial\phi_\mathrm{e}(x,y,z,t)}{\partial n} = -J_\mathrm{m}(x,y,z,t), \quad \forall(x,y,z) \in \text{any membrane}, \tag{2b}$$

$$|\phi_\mathrm{i}(x,y,z,t)| < \infty, \qquad \forall(x,y,z) \in \text{any intracellular space}, \tag{2c}$$

$$|\phi_\mathrm{e}(x,y,z,t)| < \infty \qquad \forall(x,y,z) \in \text{the extracellular space}. \tag{2d}$$

Here, $\frac{\partial}{\partial n}$ represents the derivative in the direction outwardly normal to the membrane surface. There may be other boundary conditions describing electrodes or insulating boundaries that are unnecessary to consider here and are omitted. In addition, the current density through the membrane, J_m, is the sum of resistive and capacitive components. In the subthreshold regime, in which the membrane behaviour can be assumed to be linear and modeled by an RC-circuit [38], the relationship between the membrane current density and the membrane potential is given by

$$J_\mathrm{m} = C_\mathrm{m}\frac{dV_\mathrm{m}}{dt} + \frac{V_\mathrm{m}}{R_\mathrm{m}}, \tag{3}$$

where

$$V_\mathrm{m}(x,y,z,t) \triangleq \phi_\mathrm{i}(x,y,z,t) - \phi_\mathrm{e}(x,y,z,t), \quad \forall(x,y,z) \in \text{a membrane}, \tag{4}$$

and C_m and R_m are the specific membrane capacitance and specific passive membrane resistance, respectively.

2.2. Self-consistent Volume Conductor Model for a Fibre Bundle

In this section, we derive a volume conductor model that can be used to calculate both the extracellular potential and the extracellular current density. Subsequently, either quantity can be applied as a boundary condition to calculate a consistent function for the subthreshold membrane potential using the neurite equations that have been derived previously [11, 25, 39] but are repeated in Section 3 for convenience (see Table 3). The derivation of the equations for a neurite is given in [25].

The volume conductor model is derived using a mean-field approximation comprising coupled cellular elements. To this end, the model tissue can be regarded as a composite of the neurite plus thin extracellular sheath (NTES) elements joined

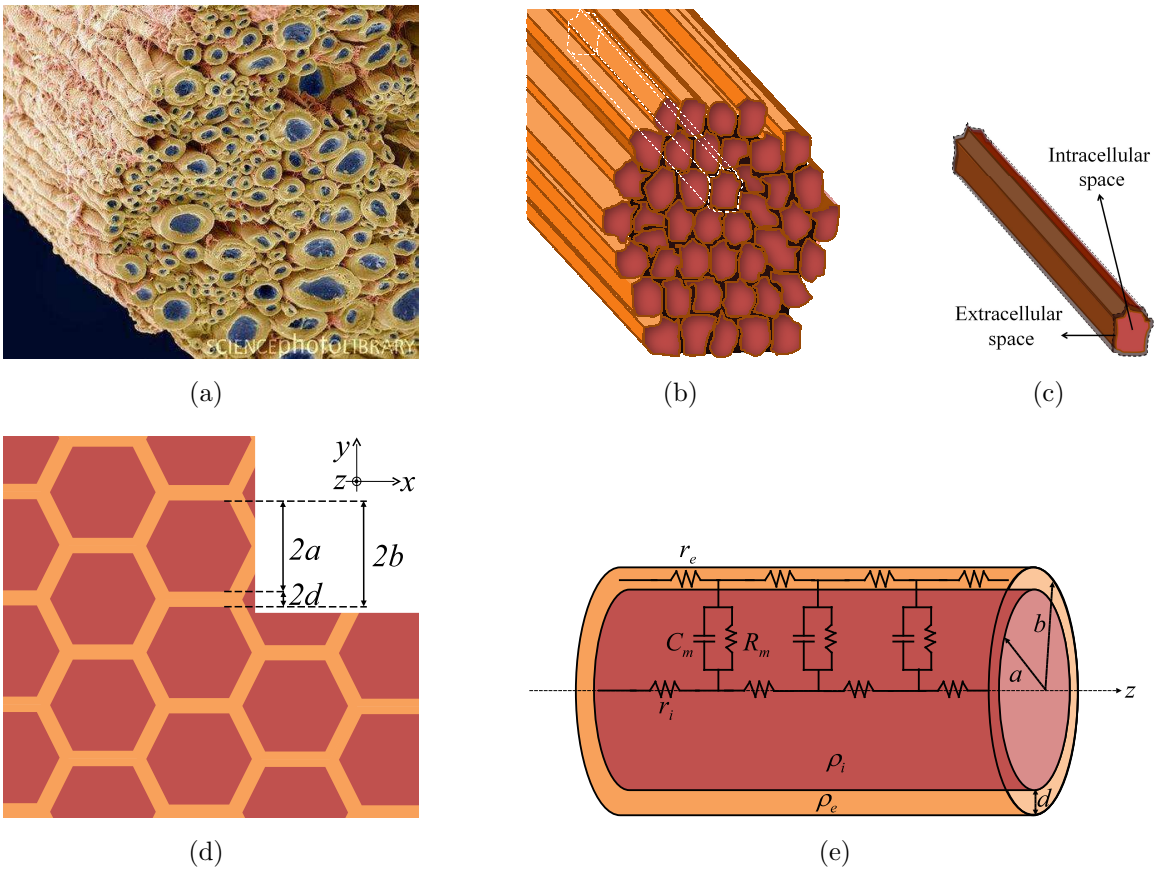

Figure 2. (a) An electron micrograph of a fibre bundle [figure is taken from Science Photo Library], (b) a conceptualised model of a fibre bundle consisting of parallel neurites with thin extracellular sheath, (c) one neurite with its extracellular space extracted from the neural tissue, (d) cross section of an idealised fibre bundle in which neurites have hexagonal cross-section. The hexagonal form is shown only for illustrative purposes to demonstrate a close packing of identical fibres, but is not an essential part of the model, (e) approximating a neurite with cylindrical intracellular and extracellular space and its equivalent electrical circuit.

along sections of their boundaries. Figure 2(b) shows a conceptualised version of a fibre bundle that consists of a composite of NTES elements in which one NTES has been highlighted (white dashed line) and extracted in Figure 2(c). As an example, a cross-section of an idealised fibre bundle that allows close packing of parallel neurites that have hexagonal cross sections is demonstrated in Figure 2(d). The electrical properties of an NTES are approximated using a cylindrical geometry, which is an appropriate approximation for neurites, with its electrical equivalent circuit in subthreshold regime is shown in Figure 2(e). The half-width of the NTES (or radius for a perfect cylinder) is $b = a + d$, where a is the half-width of intracellular space and d is the thickness of the extracellular sheath.

To explicitly redefine the fundamental model, described in the previous subsection, in terms of a system of coupled NTES elements, we first define the extracellular potential

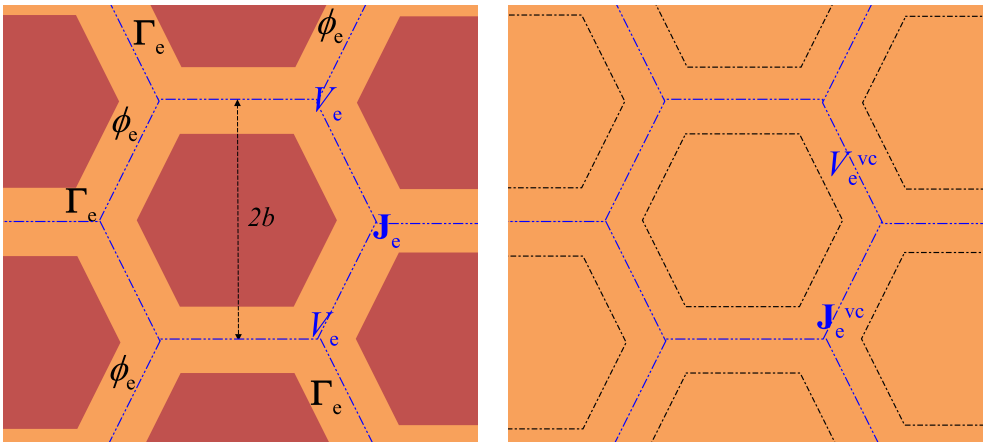

(a) (b)

Figure 3. (a) Scaled version of Figure 2(d) with boundaries shown for NTES elements in blue dash-dot-dot lines. While ϕ_e and $\mathbf{\Gamma}_e$ are defined for all points in extracellular space, V_e and $\mathbf{J}_e$ are equal to ϕ_e and $\mathbf{\Gamma}_e$ on the boundary of each neurite, respectively. (b) The neurites in neural tissue are replaced by a non-local anisotropic volume conductor to extract the extracellular potential, V_e^{vc}, or the current density, $\mathbf{J}_e^{vc}$. The black dash-dot lines indicate the location of the intracellular space of the neurite which does not exist in the volume conductor approximation. Scalar and vector fields V_e^{vc} and $\mathbf{J}_e^{vc}$ extracted from the volume conductor model in (b) are equal to V_e and $\mathbf{J}_e$ on the boundaries of the NTES elements shown by blue dash-dot-dot lines in (a).

and current density on the outer boundary of any NTES to be

$$V_e \triangleq \phi_e|_{\text{NTES boundary}}, \tag{5a}$$

$$\mathbf{J}_e \triangleq \mathbf{\Gamma}_e|_{\text{NTES boundary}}. \tag{5b}$$

To clarify, ϕ_e and $\mathbf{\Gamma}_e$ are the potential and current density, respectively, at any point in extracellular space while V_e and $\mathbf{J}_e$ are the potential and current density at points on the combined surface of the extracellular space of all NTES elements, respectively, as shown by the blue lines in Figure 3(a).

While we could label each NTES element with an integer, along with its potentials ϕ_i and ϕ_e, this notation is unnecessary in the following. Similarly, we could label the shared NTES boundaries together with their corresponding V_e and $\mathbf{J}_e$, but choose not to for simplicity. Viewing each NTES element in isolation, the intra- and extracellular potentials, ϕ_i and ϕ_e, at any point inside the NTES obey the same set of partial differential equations and boundary conditions as described by Equations (1)-(4). Additionally, in order for each NTES system to have a (unique) solution in isolation, ϕ_e must obey a boundary condition on the outer sheath of the NTES, which can be stipulated in terms of either the extracellular potential or the extracellular current

density:

$$\phi_{\mathrm{e}}(x,y,z,t) = V_{\mathrm{e}}(x,y,z,t), \qquad \forall (x,y,z) \in \text{outer NTES boundary}, \tag{6a}$$

$$\frac{\partial \phi_{\mathrm{e}}(x,y,z,t)}{\partial n} = -\rho_{\mathrm{e}} \mathbf{J}_{\mathrm{e}} \cdot \mathbf{n}(x,y,z,t), \quad \forall (x,y,z) \in \text{outer NTES boundary}, \tag{6b}$$

where $\mathbf{n}$ is the outward normal vector. Thus, we have a set of partial differential equations (PDE) and boundary conditions (BC) in three spatial and one temporal dimension for each NTES. Together, these form a system of partial differential equations and boundary conditions for the whole model of tissue (i.e., PDEs in Equations (1)-(4) and BC in Equations (6)). For any individual NTES element described by Equations (1-4), we have previously shown in [25] how to derive simpler differential equations for V_{m} in at most one spatial and one temporal dimension, given boundary conditions in terms of either V_{e}, described by Equation (6a) or $\mathbf{J}_{\mathrm{e}} \cdot \mathbf{n}$ described by Equation (6b), i.e., Stage 2 in the volume conductor approach. Explicitly, these differential equations are the cable equation for the longitudinal mode of polarisation, and ordinary differential equations in time for transverse modes. Thus, the problem of finding V_{m} throughout the tissue becomes one of NTES elements, coupled together on the shared outer NTES boundaries via V_{e} and $\mathbf{J}_{\mathrm{e}}$, which must be found self-consistently (i.e. equivalent to Stage 1 in the volume conductor approach).

The electrical properties of the NTES, captured in the partial differential equations and boundary conditions, dictate that, on the outer boundary of the sheath, $\mathbf{J}_{\mathrm{e}}$ and V_{e} must be related by a transimpedance equation. In fact, a fundamental theorem of electrical impedance tomography states that the transimpedance equations on the boundary capture all the internal electrical impedance properties of the NTES, including their geometric arrangement, provided some mild conditions are satisfied on the smoothness of the potential and the integrability of the admittivity (see [35] and references contained therein, especially Section 4). Consequently, as we are only interested in the extracellular potential, V_{e}, or current density, $\mathbf{J}_{\mathrm{e}}$, on the boundaries between NTES elements for our Stage 1 volume conductor model, we can replace Equations (1b)-(4) and Equation (6) for the intracellular potential and membrane potential with the transimpedance equations for the NTES. That is, the effect of the membrane and intracellular current paths is captured in the transimpedance. The equivalent system for V_{e} is such that

(A1) V_{e} is related to J_{e} via the transimpedance equations of the NTES.

(A2) J_{e} is locally conserved.

To derive a self-consistent mean-field approximation for the extracellular potential, we assume some additional statements, the first of which is

(A3) The transimpedance of the NTES is well approximated as though they were identical cylinders with radius b and extracellular sheath d.

The transimpedance equations for a cylindrical NTES element were derived in [25]. They are given in terms of a cylindrical coordinate system (r, z, θ, t), for which $r = b$

Table 1. Fourier transform notations.

Signal	F.T. Notation	F.T. Equation	Inverse F.T. Equation
$f(z)$	$\check{f}(k_z) = \mathcal{F}\{f(z)\}(k_z)$	$\check{f}(k_z) = \frac{1}{\sqrt{2\pi}} \int_z f(z) e^{-jk_z z} dz$	$f(z) = \frac{1}{\sqrt{2\pi}} \int_{k_z} \check{f}(k_z) e^{jk_z z} dk_z$
$g(\theta)$	$\bar{g}(n) = \mathcal{F}\{g(\theta)\}(n)$	$\bar{g}(n) = \frac{1}{2\pi} \int_{2\pi} g(\theta) e^{-jn\theta} d\theta$	$g(\theta) = \sum_{n=-\infty}^{+\infty} \bar{g}(n) e^{jn\theta}$
$h(t)$	$\hat{h}(\omega) = \mathcal{F}\{h(t)\}(\omega)$	$\hat{h}(\omega) = \frac{1}{\sqrt{2\pi}} \int_t h(t) e^{-j\omega t} dt$	$h(t) = \frac{1}{\sqrt{2\pi}} \int_{\omega} \hat{h}(\omega) e^{j\omega t} d\omega$

on the outer surface of the sheath, so that (z, θ, t) provides a coordinate system on this boundary. The (z, θ, t) coordinates are Fourier transformed into (k_z, n, ω) coordinates, where k_z and ω are real numbers and n is an integer (see Table (1) for definitions). For a Fourier transformed cylindrical coordinate system centred at $[x, y]$, the transimpedance equations may be written as

$$\hat{\bar{V}}_{\mathrm{e}}[x, y](k_z, n, \omega) = -\hat{\bar{Z}}_{\mathrm{e}}(k_z, n, \omega)\, \hat{\bar{\mathbf{J}}}_{\mathrm{e}} \cdot \mathbf{n}[x, y](k_z, n, \omega). \tag{7}$$

Note that the equation relates trebly Fourier transformed quantities for the extracellular potential, $\hat{\bar{V}}_{\mathrm{e}}$, and the current density, $\hat{\bar{J}}_{\mathrm{e}}$, as denoted by the hat notation specified in Table 1. The transimpedance is given by

$$\hat{\bar{Z}}_{\mathrm{e}}(k_z, n, \omega) = \begin{cases} \dfrac{2\pi b r_{\mathrm{e}} r_{\mathrm{i}} \Big(1 + j\omega\tau_{\mathrm{m}} + k_z^2 \lambda_{0_{\mathrm{V}}}^2\Big)}{k_z^2 (r_{\mathrm{e}} + r_{\mathrm{i}}) \Big(1 + j\omega\tau_{\mathrm{m}} + k_z^2 \lambda_{0_{\mathrm{J}}}^2\Big)}, & n = 0 \\ \dfrac{R_{\mathrm{e},J}(n) \Big(Z_{\mathrm{m}}(\omega) + R_{\mathrm{i},V}(n) + R_{\mathrm{e},V}(n)\Big)}{Z_{\mathrm{m}}(\omega) + R_{\mathrm{e},J}(n) + R_{\mathrm{i},J}(n)} \approx \dfrac{\rho_{\mathrm{e}} b^2}{n^2 d}, & n \neq 0. \end{cases} \tag{8}$$

where the expressions for $\lambda_{0_{\mathrm{V}}}$, $\lambda_{0_{\mathrm{J}}}$, r_{i}, r_{e}, Z_{m}, $R_{\mathrm{i},V}(n)$, $R_{\mathrm{e},V}(n)$, $R_{\mathrm{e},J}(n)$ and $R_{\mathrm{i},J}(n)$ (in terms of previously defined fundamental parameters) are given in Table 2 along with their physical interpretation.

The discrete values of $n = 0, 1, 2, \ldots$ can be interpreted as the different modes of stimulation as depicted in Figure 1. The $n = 0$ mode is the longitudinal mode and corresponds to current passing into the NTES in a rotationally symmetric fashion and passing along the neurite both extra- and intracellularly as shown in Figure 1(a). It corresponds to the classic mode of neural polarisation described by the cable equation. The $n = 1$ mode corresponds to a transverse mode, in which current passes directly across the NTES as illustrated in Figure 1(b). The passing current polarises opposite sides of the neurite in an opposite fashion; i.e., depolarised on one side and hyperpolarised on the other. The higher order modes, $n \geq 2$, are also transverse, but have higher order symmetries as shown in Figure 1(c) for $n = 2$. Generally, the

Table 2. Parameters used in equations governing the membrane potential for different modes of stimulation under current density and voltage boundary conditions.

Parameter	Name	Expression
r_{i}	Intracellular resistance per unit length	$\frac{\rho_{\mathrm{i}}}{\pi a^2}$
r_{e}	Extracellular resistance per unit length	$\frac{\rho_{\mathrm{e}}}{\pi(b^2-a^2)} \approx \frac{\rho_{\mathrm{e}}}{2\pi bd}$
$R_{\mathrm{i,J}}(n)$	Transverse intracellular specific resistance for $\mathbf{J}_{\mathrm{e}}$ BC	$\frac{\rho_{\mathrm{i}} b}{\lvert n\rvert}$
$R_{\mathrm{e,J}}(n)$	Transverse extracellular specific resistance for $\mathbf{J}_{\mathrm{e}}$ BC	$\frac{\rho_{\mathrm{e}} b^2}{n^2 d}$
$R_{\mathrm{i,V}}(n)$	Transverse intracellular specific resistance for V_{e} BC	$\frac{\rho_{\mathrm{i}} b}{\lvert n\rvert}$
$R_{\mathrm{e,V}}(n)$	Transverse extracellular specific resistance for V_{e} BC	$\rho_{\mathrm{e}} d$
Z_{m}	Specific membrane impedance	$\left(\frac{1}{R_{\mathrm{m}}} + j\omega C_{\mathrm{m}}\right)^{-1}$
r_{m}	Membrane unit length resistance	$\frac{R_{\mathrm{m}}}{2\pi a} \approx \frac{R_{\mathrm{m}}}{2\pi b}$
z_{m}	Membrane unit length impedance	$\frac{Z_{\mathrm{m}}}{2\pi a} \approx \frac{Z_{\mathrm{m}}}{2\pi b}$
τ_{L}	Longitudinal time constant equal to the membrane time constant	$R_{\mathrm{m}} C_{\mathrm{m}}$
$\tau_{\mathrm{T_J}}$	Transverse time constant for $\mathbf{J}_{\mathrm{e}}BC$	$\left(\frac{1}{R_{\mathrm{m}}} + \left(R_{\mathrm{i,J}}(n) + R_{\mathrm{e,J}}(n)\right)^{-1}\right)^{-1} C_{\mathrm{m}}$
$\tau_{\mathrm{T_V}}$	Transverse time constant for $V_{\mathrm{e}}BC$	$\left(\frac{1}{R_{\mathrm{m}}} + \frac{1}{R_{\mathrm{i,V}}(n)+R_{\mathrm{e,V}}(n)}\right)^{-1} C_{\mathrm{m}}$
$\lambda_{0_{\mathrm{J}}}$	Static electrotonic length constant for $\mathbf{J}_{\mathrm{e}}BC$	$\sqrt{\frac{r_{\mathrm{m}}}{r_{\mathrm{e}}+r_{\mathrm{i}}}}$
$\lambda_{\mathrm{J}}(\omega)$	Frequency dependent electrotonic length constant for $\mathbf{J}_{\mathrm{e}}$ BC	$\frac{\lambda_{0_{\mathrm{J}}}}{\sqrt{1+j\omega\tau_{\mathrm{L}}}} = \sqrt{\frac{z_{\mathrm{m}}}{r_{\mathrm{e}}+r_{\mathrm{i}}}}$
$\lambda_{0_{\mathrm{V}}}$	Static electrotonic length constant for $V_{\mathrm{e}}BC$	$\sqrt{\frac{r_{\mathrm{m}}}{r_{\mathrm{i}}}}$
$\lambda_{\mathrm{V}}(\omega)$	Frequency dependent electrotonic length constant for $V_{\mathrm{e}}BC$	$\frac{\lambda_{0_{\mathrm{V}}}}{\sqrt{1+j\omega\tau_{\mathrm{L}}}} = \sqrt{\frac{z_{\mathrm{m}}}{r_{\mathrm{i}}}}$

extracellular potential is a superposition of all these modes, but typically the first two modes dominate.

We make the following additional key mean-field assumption to derive the cellular composite volume conductor equations:

(A4) The transimpedance equation holds for *any* cylinder of radius b with its axis in the z-direction for $n = 0$ and $n = 1$ modes. The $n = 2, 3, \ldots$ modes contribute negligibly to the electrical properties of the tissue.

The assumption that the transimpedance equation holds for any cylinder of the correct size and orientation essentially replaces the discrete set of NTES elements with a homogeneous volume conductor with specific impedance chosen to provide a match to the first two modes of the NTES element. Figures 3(a) and 3(b) graphically depict how neural tissue with its neurites will be replaced with a volume conductor. In this sense, the assumption amounts to spatially averaging over the fine structure of the NTES. However, the dominant effects of a neurite's electrical properties, geometry and packing with respect to other cells are retained through the first two modes of the NTES transimpedance. Notice that the assumption also guarantees that the resulting volume conductor model will give self-consistent answers for membrane potential, provided we are only interested in the $n = 0$ longitudinal and $n = 1$ transverse modes.

To derive the constitutive equation for the cellular composite volume conductor model, the transimpedance Equation (8) must be transformed from the (k_z, n, ω) coordinate system, which is the Fourier transformed local cylindrical coordinate system of any cylinder with axis at $[x, y]$, to the (x, y, z, t) global cartesian coordinate system. This can be done by first approximating V_e and $\mathbf{J}_\mathrm{e}$ on the surface of a cylinder at $(\tilde{x} = x + b\cos\theta, \tilde{y} = y + b\sin\theta, \tilde{z} = z)$ using a Taylor expansion in terms of b and performing the Fourier θ-transform to calculate $\bar{V}_\mathrm{e}[x, y](z, n, t)$ and $\bar{\mathbf{J}}_\mathrm{e} \cdot \mathbf{n}[x, y](z, n, t)$ in terms of $V_\mathrm{e}(x, y, z, t)$ and $\mathbf{J}_\mathrm{e}(x, y, z, t)$ (see Appendix A). This gives the relations

$$\bar{V}_\mathrm{e}[x, y](z, 0, t) = V_\mathrm{e}(x, y, z, t), \tag{9a}$$

$$\bar{\mathbf{J}}_\mathrm{e}^\mathrm{vc} \cdot \mathbf{n}[x, y](z, 0, t) = \frac{-b}{2} \frac{\partial J_{\mathrm{e},z}(x, y, z, t)}{\partial z}, \tag{9b}$$

$$\bar{V}_\mathrm{e}[x, y](z, 1, t) = \frac{b}{2} \left(\frac{\partial V_\mathrm{e}(x, y, z, t)}{\partial x} - j \frac{\partial V_\mathrm{e}(x, y, z, t)}{\partial y} \right), \tag{9c}$$

$$\bar{\mathbf{J}}_\mathrm{e}^\mathrm{vc} \cdot \mathbf{n}[x, y](z, 1, t) = \frac{1}{2} \Big(J_{\mathrm{e},x}(x, y, z, t) - j J_{\mathrm{e},y}(x, y, z, t) \Big). \tag{9d}$$

The superscript "vc" for $\mathbf{J}_\mathrm{e}^\mathrm{vc}$ indicates that this current density pertains to the cellular composite volume conductor model and is required to distinguish it from the extracellular current density of the bidomain model, which is introduced later. The extracellular potential, V_e, does not require this superscript because it is identical to the bidomain extracellular potential. This issue will be discussed further in Section 4. The above equations can be Fourier transformed into the (k_z, ω) domain to re-express the transimpedance Equation (7) in terms of $V_\mathrm{e}(x, y, k_z, \omega)$ and $\mathbf{J}_\mathrm{e}(x, y, k_z, \omega)$ (see Appendix A). Performing the inverse Fourier transform back to the (z, t) domain gives the

constitutive equation (Equation (10a)), (see Analytical Results section). The local conservation of the current density (Assumption (A2)) gives the continuity equation (Equation (10b)), which completes the derivation of the cellular composite volume conductor model.

3. Analytic Results

In this section, the equations governing the extracellular potential, V_e, and current density, $\mathbf{J}_\mathrm{e}$, are given for cellular composite models. For completeness, equations for the membrane potential are also given, although these are not new. We first give the equations for the cellular composite volume conductor model in the case of tissue comprising identical parallel fibres; next, the equivalent bidomain equations are given; finally, the equations for both volume conductor and multidomain cellular composite models are given for very general tissue types including mixtures of different cell types with arbitrarily crossing fibres.

3.1. Cellular Composite Volume Conductor Model for Identical Parallel Fibres

3.1.1. Stage 1 The equations describing the extracellular potential and current density for the cellular composite volume conductor models, in the case of identical parallel fibres, are

$$\mathbf{J}_\mathrm{e}^\mathrm{vc} = -\frac{1}{2\pi}\boldsymbol{\xi}_\mathrm{e}^\mathrm{vc} \underset{z,t}{*} \boldsymbol{\nabla} V_\mathrm{e}, \qquad \text{Constitutive Equation,} \tag{10a}$$

$$\boldsymbol{\nabla}\cdot\mathbf{J}_\mathrm{e}^\mathrm{vc} = 0, \qquad \text{Continuity Equation.} \tag{10b}$$

The convolution, denoted by "$*$", in Equation (10a) occurs over both time and space in the z-direction and is a novel aspect of the model (cf. simple multiplication in the standard volume conductor case $\mathbf{J}_\mathrm{e} = -\sigma V_\mathrm{e}$; the factor of $1/2\pi$ in Equation (10a) arises from the convolution due to our definition of the Fourier transform). Here, convolution is defined as $f \underset{z,t}{*} g = \int_{-\infty}^{\infty} dz' \int_{-\infty}^{\infty} dt' f(z',t') g(z-z', t-t')$. The derivation of the constitutive equation is outlined in the Methods section with additional details presented in Appendix B. The extracellular admittivity kernel for the volume conductor model is

$$\boldsymbol{\xi}_\mathrm{e}^\mathrm{vc}(z,t) = \begin{bmatrix} \xi_{\mathrm{e,T}}^\mathrm{vc}(z,t) & 0 & 0 \\ 0 & \xi_{\mathrm{e,T}}^\mathrm{vc}(z,t) & 0 \\ 0 & 0 & \xi_{\mathrm{e,L}}^\mathrm{vc}(z,t) \end{bmatrix}, \tag{11}$$

where

$$\xi_{\mathrm{e,T}}^\mathrm{vc}(z,t) = 2\pi\sigma_{\mathrm{e,T0}}^\mathrm{vc}\delta(z)\delta(t) = \frac{2\pi d}{b\rho_\mathrm{e}}\delta(z)\delta(t), \tag{12a}$$

$$\xi_{\mathrm{e,L}}^\mathrm{vc}(z,t) = \frac{2\pi\delta(z)\delta(t)}{\rho_\mathrm{i}} - \frac{\sqrt{\pi}H(t)\tau_\mathrm{L}^{\frac{3}{2}}}{4\rho_\mathrm{i}\lambda_{0\mathrm{V}}t^{\frac{5}{2}}}\left(\frac{2t}{\tau_\mathrm{L}} - \frac{z^2}{\lambda_{0\mathrm{V}}^2}\right) e^{-\left(\frac{t}{\tau_\mathrm{L}} + \frac{z^2}{4\lambda_{0\mathrm{V}}^2}\frac{\tau_\mathrm{L}}{t}\right)}, \tag{12b}$$

in which $\xi^{\mathrm{vc}}_{\mathrm{e,T}}$ and $\xi^{\mathrm{vc}}_{\mathrm{e,L}}$ are the transverse and longitudinal components of the admittivity kernel, respectively, and $H(t)$ is the Heaviside function. The terms involving delta functions are parts of the admittivity kernel that reduce to standard multiplicative conductivity once the convolution is performed. The non-trivial part of the admittivity kernel is contained in its longitudinal component, which is given by Equation (12b), excluding the delta function term, to demonstrate the (non-trivial) spatio-temporal filtering properties of tissue that result from its cellular composition.

In principle, one can substitute Equation (10a) into Equation (10b) to obtain a second-order integro-partial differential equation for V_{e}, which could be solved given appropriate boundary conditions. $\mathbf{J}^{\mathrm{vc}}_{\mathrm{e}}$ could then be found via back substitution into Equation (10a). In practice, the integro-partial differential equation is non-trivial to solve, especially given the complicated form of $\xi^{\mathrm{vc}}_{\mathrm{e,L}}(z,t)$. A useful alternative when dealing with problems that can be approximated to have infinite extent in the direction to the fibres is to rewrite Equations (10) and (11) in the (k_z,ω)-Fourier domain, which changes the convolution in Equation (10a) to multiplication and simplifies the expression for extracellular admittivity,

$$\hat{\check{\mathbf{J}}}_{\mathrm{e}} = -\hat{\check{\boldsymbol{\xi}}}^{\mathrm{vc}}_{\mathrm{e}}\check{\boldsymbol{\nabla}}\hat{\check{V}}_{\mathrm{e}}, \tag{13a}$$

$$\check{\boldsymbol{\nabla}}\cdot\hat{\check{\mathbf{J}}}_{\mathrm{e}} = 0, \tag{13b}$$

$$\hat{\check{\xi}}^{\mathrm{vc}}_{\mathrm{e,T}}(k_z,\omega) = \sigma^{\mathrm{vc}}_{\mathrm{e,T0}} = \frac{d}{b\rho_{\mathrm{e}}}, \tag{13c}$$

$$\hat{\check{\xi}}^{\mathrm{vc}}_{\mathrm{e,L}}(k_z,\omega) = \frac{1}{\rho_{\mathrm{i}}}\left(\frac{1+j\omega\tau_{\mathrm{m}}+k_z^2\lambda_{0_J}^2}{1+j\omega\tau_{\mathrm{m}}+k_z^2\lambda_{0_V}^2}\right). \tag{13d}$$

We refer to $\xi^{\mathrm{vc}}_{\mathrm{e},}$ as the admittivity kernel and its Fourier transformed equivalent $\hat{\check{\boldsymbol{\xi}}}^{\mathrm{vc}}_{\mathrm{e}}$ as the admittivity. Here, $\check{\boldsymbol{\nabla}} \triangleq [\partial/\partial x, \partial/\partial y, jk_z]$, which is the Fourier transform in terms of z for the operator $\boldsymbol{\nabla}$ defined as a column vector. Consequently, the set of Equations (13) give a partial differential equation in two-dimensions (x,y) for $\hat{\check{V}}_{\mathrm{e}}(x,y,k_z,\omega)$.

3.1.2. Stage 2 Once the extracellular potential, V_{e}, is obtained (Stage 1), the longitudinal and transverse components of the membrane potential can be calculated using the following respective equations (Stage 2) [25],

$$\lambda_{0_{\mathrm{V}}}^2\frac{\partial^2 V_{\mathrm{m,L}}(z,t)}{\partial z^2} - \tau_{\mathrm{L}}\frac{\partial V_{\mathrm{m,L}}(z,t)}{\partial t} - V_{\mathrm{m,L}}(z,t) = -\lambda_{0_{\mathrm{V}}}^2\frac{\partial^2 V_{\mathrm{e}}(z,t)}{\partial z^2}, \tag{14a}$$

$$\tau_{\mathrm{T_V}}\frac{dV^{\mathrm{Max}}_{\mathrm{m,T}}(z,t)}{dt} + V^{\mathrm{Max}}_{\mathrm{m,T}}(z,t) = -\left(\frac{R_{\mathrm{m}}}{R_{\mathrm{m}}+R_{\mathrm{i,V}}(n)+R_{\mathrm{e,V}}(n)}\right)V_{\mathrm{e,T}}(z,t), \qquad n\neq 0. \tag{14b}$$

where

$$V^{\mathrm{Max}}_{\mathrm{m,T}}(z,t) \triangleq \max_{\theta}\{V_{\mathrm{m,T}}(z,\theta,t)\}, \tag{15}$$

Table 3. Equations for membrane potential under different boundary conditions.

	Membrane potential equations for voltage boundary condition
$n=0$	$\lambda_{0_{\rm V}}^2 \frac{\partial^2 V_{\rm m,L}(z,t)}{\partial z^2} - \tau_{\rm L} \frac{\partial V_{\rm m,L}(z,t)}{\partial t} - V_{\rm m,L}(z,t) = -\lambda_{0_{\rm V}}^2 \frac{\partial^2 V_{\rm e}(z,t)}{\partial z^2}$
$n=1$	$\tau_{\rm T_V} \frac{dV_{\rm m,T}^{\rm Max}(z,t)}{dt} + V_{\rm m,T}^{\rm Max}(z,t) = -\left(\frac{R_{\rm m}}{R_{\rm m}+R_{\rm i,V}(1)+R_{\rm e,V}(1)}\right) V_{\rm e,T}(z,t)$
	Membrane potential equations for current density boundary condition
$n=0$	$\lambda_{0_{\rm J}}^2 \frac{\partial^2 V_{\rm m,L}(z,t)}{\partial z^2} - \tau_{\rm L} \frac{\partial V_{\rm m,L}(z,t)}{\partial t} - V_{\rm m,L}(z,t) = \frac{\rho_e b}{2d} \lambda_{0_{\rm J}}^2 \frac{\partial J_{\rm e,z}^{\rm vc}}{\partial z}$
$n=1$	$\tau_{\rm T_J} \frac{dV_{\rm m,T}^{\rm Max}(z,t)}{dt} + V_{\rm m,T}^{\rm Max}(z,t) = \left(\frac{R_{\rm e,J}(1) R_{\rm m}}{R_{\rm m}+R_{\rm i,J}(1)+R_{\rm e,J}(1)}\right) J_{\rm e,T}(z,t)$

and

$$V_{\rm e,T}(z,t) \triangleq b|\boldsymbol{\nabla}_{\rm T} V_{\rm e}(z,t)|, \tag{16}$$

$\tau_{\rm L}$, $\tau_{\rm T_V}$, $R_{\rm i,V}(n)$ and $R_{\rm e,V}(n)$ are given in Table 2. $V_{\rm m,L}(z,t)$ and $V_{\rm m,T}(z,t)$ are the longitudinal and transverse components of the membrane potential and $\boldsymbol{\nabla}_{\rm T} \triangleq [\partial/\partial x, \partial/\partial y]$. Alternatively, one can calculate the membrane potential using the extracellular current density, $\mathbf{J}_{\rm e}^{\rm vc}$, using an analogous pair of equations given in Table 3. In this table

$$J_{\rm e,T}(z,t) \triangleq 2|\bar{\mathbf{J}}_{\rm e}[\tilde{x},\tilde{y}](z,1,t)\cdot\mathbf{n}| = |[J_{{\rm e},x}(z,t),\ J_{{\rm e},y}(z,t)]|. \tag{17}$$

The self-consistency of the cellular composite volume conductor ensures that the results will be the same regardless of which type of boundary conditions are used for the dominant, $n=0$ longitudinal and $n=1$ transverse, component of the membrane potential.

It is also possible to express Eqsuations (14) for the membrane potential in the (k_z,ω) Fourier domain. For the longitudinal mode, this is

$$\hat{\tilde{V}}_{\rm m,L} = -\frac{k_z^2 \lambda_{\rm V}^2(\omega)}{1+k_z^2\lambda_{\rm V}^2(\omega)} \hat{\tilde{V}}_{\rm e}. \tag{18}$$

This representation for membrane potential is useful when the volume conductor model has also been solved for $V_{\rm e}$ or $\mathbf{J}_{\rm e}^{\rm vc}$ in the (k_z,ω)-Fourier domain. As an example, Equations (13) and (14) are solved in the Fourier domain for the case of a point source electrode in a bundle of fibres that extend infinitely in all direction in the companion paper. A comparison to point source solutions with standard volume conductor models is given.

A complete set of equation for extracellular current density and potential and for the membrane potential with either voltage or current density boundary conditions

are summarised in Tables C1 and C2 in Appendix C for the (k_z, ω), (k_z, t) and (z, ω) representations, as well as the (z, t) case.

3.2. Bidomain Model for Tissue Composed of Identical Parallel Fibres

The volume conductor model described in the previous section is mathematically equivalent to a bidomain model, which is presented in this section. The proof of this is given in Appendix D. One of the main advantages of using the bidomain formulation is that it is relatively straight-forward to implement in standard finite element modelling packages such as COMSOL and ANSYS. This allows one to obtain numerical solutions to problems with geometries and boundary conditions where no analytic solution is forthcoming.

Bidomain models provide an approximation to the electrical properties of tissue by using both intracellular and extracellular continua that are electrically conductive and coincident in space. The intra- and extracellular continua (alternatively known as domains) are coupled together via a membrane that permits current flow across it. The membrane is also taken to be continuously present throughout the space occupied by the bidomain model [40]. By contrast to the volume conductor models, V_e and V_m are calculated together in a single stage.

The model can be defined in terms of the current densities in the intracellular domain, the extracellular domain and through the membrane,

$$\mathbf{J}_\mathrm{i}^\mathrm{bd} = -\boldsymbol{\sigma}_\mathrm{i}^\mathrm{bd} \boldsymbol{\nabla} V_\mathrm{i}, \tag{19a}$$

$$\mathbf{J}_\mathrm{e}^\mathrm{bd} = -\boldsymbol{\sigma}_\mathrm{e}^\mathrm{bd} \boldsymbol{\nabla} V_\mathrm{e}, \tag{19b}$$

$$J_\mathrm{m}^\mathrm{bd} = C_\mathrm{m} \frac{dV_\mathrm{m,L}}{dt} + \frac{V_\mathrm{m,L}}{R_\mathrm{m}}, \tag{19c}$$

where V_i, V_e and $V_\mathrm{m,L} \triangleq V_\mathrm{e} - V_\mathrm{i}$ are the intracellular, extracellular and longitudinal component of the membrane potential, respectively, as defined previously for the volume conductor model. The intracellular and extracellular conductivity tensors have the form

$$\boldsymbol{\sigma}_\mathrm{i}^\mathrm{bd} = \begin{bmatrix} 0 & 0 & 0 \\ 0 & 0 & 0 \\ 0 & 0 & \sigma_\mathrm{i,L}^\mathrm{bd} \end{bmatrix}, \tag{20a}$$

$$\boldsymbol{\sigma}_\mathrm{e}^\mathrm{bd} = \begin{bmatrix} \sigma_\mathrm{e,T}^\mathrm{bd} & 0 & 0 \\ 0 & \sigma_\mathrm{e,T}^\mathrm{bd} & 0 \\ 0 & 0 & \sigma_\mathrm{e,L}^\mathrm{bd} \end{bmatrix}. \tag{20b}$$

The components of the tensors are *effective* conductivities in x, y and z directions. This takes into account the cross-sectional area of current flow in each direction in each domain, as well as the intrinsic resistivity of fluid in each domain. As such, they can easily be derived by taking into account the resistivity of the intracellular or

extracellular fluid (ρ_i and ρ_e) and cross-sectional areas of intracellular or extracellular space in longitudinal or transverse directions based on the cylindrical NTES element of outer radius b and inner radius a:

$$\sigma_{\mathrm{i,L}}^{\mathrm{bd}} = \frac{\pi a^2}{\pi b^2 \rho_\mathrm{i}} \approx \frac{1}{\rho_\mathrm{i}}, \qquad \text{for } d \ll b, \tag{21a}$$

$$\sigma_{\mathrm{e,L}}^{\mathrm{bd}} = \frac{\pi b^2 - \pi a^2}{\pi b^2 \rho_\mathrm{e}} \approx \frac{2d}{b\rho_\mathrm{e}}, \qquad \text{for } d \ll b, \tag{21b}$$

$$\sigma_{\mathrm{e,T}}^{\mathrm{bd}} = \frac{b}{R_{\mathrm{e},J}} = \frac{d}{b\rho_\mathrm{e}}, \qquad \text{for } d \ll b. \tag{21c}$$

The requirement that $d \ll b$ is typically a good approximation due to the confined extracellular space, so that d is in the range of tens of nanometers, while b is in the range of hundreds of nanometers for axons and micrometers for dendrites. One must also define the membrane surface area to volume ratio, β, in order to define the amount of current entering or leaving a domain via the membrane surface,

$$\beta \triangleq \frac{\text{Membrane surface area}}{\text{Neurite volume}} = \frac{2\pi a L}{\pi a^2 L} \approx \frac{2}{b}, \tag{22}$$

where L is some arbitrary length of cylinder.

With these definitions, the bidomain equations may be stated as

$$\boldsymbol{\nabla} \cdot \mathbf{J}_\mathrm{i}^{\mathrm{bd}} + \beta \mathbf{J}_\mathrm{m}^{\mathrm{bd}} = \mathbf{0}, \tag{23a}$$

$$\boldsymbol{\nabla} \cdot \mathbf{J}_\mathrm{e}^{\mathrm{bd}} - \beta \mathbf{J}_\mathrm{m}^{\mathrm{bd}} = \mathbf{0}, \tag{23b}$$

which is the result of the conservation of total current across the two domains at every point. In terms of coupled partial differential equations for the intracellular and extracellular potential, these equations may be written as

$$\sigma_{\mathrm{i,L}}^{\mathrm{bd}} \frac{\partial^2 V_\mathrm{i}}{\partial z^2} - \beta \left(C_\mathrm{m} \frac{dV_{\mathrm{m,L}}}{dt} + \frac{V_{\mathrm{m,L}}}{R_\mathrm{m}} \right) = 0, \tag{24a}$$

$$\sigma_{\mathrm{e,T}}^{\mathrm{bd}} \frac{\partial^2 V_\mathrm{e}}{\partial x^2} + \sigma_{\mathrm{e,T}}^{\mathrm{bd}} \frac{\partial^2 V_\mathrm{e}}{\partial y^2} + \sigma_{\mathrm{e,L}}^{\mathrm{bd}} \frac{\partial^2 V_\mathrm{e}}{\partial z^2} + \beta \left(C_\mathrm{m} \frac{dV_{\mathrm{m,L}}}{dt} + \frac{V_{\mathrm{m,L}}}{R_\mathrm{m}} \right) = 0. \tag{24b}$$

The longitudinal part of the membrane potential is calculated directly in the bidomain model. The transverse part must be found, once V_e is calculated, using Equation (14b).

3.3. Extension to General Tissue Compositions

The foregoing sections assumed that the tissue was a fibre bundle composed of closely packed, identical neurites with parallel orientation. While there are many instances in the nervous system of bundles of axons oriented in parallel, they are not necessarily identical, especially in their diameters. Furthermore, many tissues in the nervous system consist of neurites that are crossing, have different diameters and/or specific membrane

resistance (e.g. cortical gray matter). The tissue may also include glial cells that, like neurons, also have a dendritic structure that may be approximated using cylindrical elements. In general, the tissue is extremely closely packed, with a highly confined extracellular space, that is well modelled as a collection of coupled NTES elements.

Deriving a volume conductor model from first principles for such a complex model of tissue is very difficult. However, based on the results for the volume conductor model for identical parallel fibres, some simple generalisation can be made to support the following mean-field model.

Suppose the tissue comprises a collection of different classes of fibres (axons, dendrites of neurons and glia), with each class having its own orientation, diameter and membrane properties. Label the classes $h = 1, \ldots, H$. We assume that fibres from different classes are intermingled in an essentially random fashion, with each class occupying some fraction of the volume. Consider a small volume of tissue. For each fibre in that tissue, the extracellular current density around that fibre must be related to the extracellular potential via a transimpedance equation of a form analogous to Equation (10a),

$$\mathbf{J}^{\mathrm{vc}}_{\mathrm{e},h} = -\frac{1}{2\pi}\boldsymbol{\xi}^{\mathrm{vc}}_{\mathrm{e},h} \underset{\mathbf{u}_h,t}{*} \boldsymbol{\nabla} V_{\mathrm{e},h}, \tag{25}$$

where the admittivity kernel, $\boldsymbol{\xi}^{\mathrm{vc}}_{\mathrm{e},h}$, is of a form suitable for the fibres' orientations, diameters and membrane properties, and $\mathbf{u}_h$ represents the unit vector parallel to fibres' axes. The spatial convolution is in the direction $\mathbf{u}_h$ and so that the whole convolution is defined as $(f \underset{\mathbf{u},t}{*} g)(\mathbf{p}, t) = \int_{-\infty}^{\infty} ds' \int_{-\infty}^{\infty} dt' f(s'\mathbf{u}, t') g(\mathbf{p} - s'\mathbf{u}, t - t')$ for a point in space $\mathbf{p} = (x, y, z)$. We now assume that within a sufficiently small volume of tissue, the spatial fluctuations in extracellular potential can be neglected to a first approximation so that $V_{\mathrm{e},h}$ can be replaced by its mean value V_{e} in that small volume, the same in the vicinity of all fibre types. This mean extracellular potential is determined by the mean extracellular current density within the small volume,

$$\mathbf{J}^{\mathrm{vc}}_{\mathrm{e}} = \sum_{h=1}^{H} \alpha_h \mathbf{J}^{\mathrm{vc}}_{\mathrm{e},h}, \tag{26}$$

where α_h is the total volume fraction (i.e., the fractional volume of space occupied by that neurite class). Assuming local conservation of the mean extracellular current in this volume, we also have

$$\boldsymbol{\nabla} \cdot \mathbf{J}^{\mathrm{vc}}_{\mathrm{e}} = 0, \tag{27}$$

in the limit of a vanishingly small volume.

Equations (25)-(27), with $V_{\mathrm{e},h}$ replaced by V_{e}, define the basic equations governing the generalised cellular composite volume conductor model. Note that the transimpedance Equation (25) guarantees the self-consistent calculation of V_{m} using both voltage and current density boundary conditions provided that the fibres individual current density, $\mathbf{J}_{\mathrm{e},h}$, is used for the latter. The form of admittivity kernel, $\boldsymbol{\xi}^{\mathrm{vc}}_{\mathrm{e},h}$, for any

arbitrarily oriented fibre with axis in direction of the unit vector, $\mathbf{u}_h$, is given most simply in the full spatial and temporal Fourier domain

$$\hat{\check{\boldsymbol{\xi}}}^{\mathrm{vc}}_{\mathrm{e}}(\mathbf{k},\omega;\mathbf{u}_h) = \hat{\check{\xi}}^{\mathrm{vc}}_{\mathrm{e,T}}\mathbf{I} + (\hat{\check{\xi}}^{\mathrm{vc}}_{\mathrm{e,L}}(\mathbf{k}\cdot\mathbf{u}_h,\omega) - \hat{\check{\xi}}^{\mathrm{vc}}_{\mathrm{e,T}})\mathbf{u}_h\mathbf{u}_h^T, \tag{28a}$$

$$\hat{\check{\xi}}^{\mathrm{vc}}_{\mathrm{e,T}} = \frac{d_h}{b_h\rho_{\mathrm{e}}}, \tag{28b}$$

$$\hat{\check{\xi}}^{\mathrm{vc}}_{\mathrm{e,L}}(\mathbf{k}\cdot\mathbf{u}_h,\omega) = \frac{1}{\rho_{\mathrm{i},h}}\frac{1+j\omega\tau_{\mathrm{L},h}+(\mathbf{k}\cdot\mathbf{u}_h)^2\lambda^2_{0_{\mathrm{J}},h}}{1+j\omega\tau_{\mathrm{L},h}+(\mathbf{k}\cdot\mathbf{u}_h)^2\lambda^2_{0_{\mathrm{V}},h}}, \tag{28c}$$

where the vector $\mathbf{k}$ is the three dimensional Fourier couple of a point in space $\mathbf{p}$, $\breve{f}$ denotes the three dimensional spatial Fourier transform of f, $\mathbf{I}$ is the 3×3 identity matrix and $\mathbf{u}_h\mathbf{u}_h^T$ is the outer product of the unit column vector $\mathbf{u}_h$. Consequently, the total admittivity kernel is given by

$$\boldsymbol{\xi}^{\mathrm{vc}}_{\mathrm{e}} = \sum_{h=1}^{H}\alpha_h\boldsymbol{\xi}^{\mathrm{vc}}_{\mathrm{e}}(\mathbf{k},\omega;\mathbf{u}_h). \tag{29}$$

In practice, when h represents a continuous parameter, the sum in Equation 26 and for the total admittivity kernel become integrals. For example, if h represents orientation, the unit vector may be parameterized in term of spherical polar coordinates so that $\mathbf{u}_h = [\cos(\theta)\sin(\phi), \sin(\theta)\sin(\phi), \cos(\phi)]$. In some simple cases, the integrals can be performed analytically to provide closed form expressions for the equations governing V_{e}, while in more complicated cases, the integrals must be performed numerically.

As per the fibre bundle case, once the Stage 1 equations have been solved for extracellular quantities, the membrane potentials (one for each class of cell) may be found in Stage 2.

As an alternative, and similar to the fibre bundle case, this more general volume conductor model has a mathematically equivalent multi-domain model, with H intracellular domains and one extracellular domain. It is determined by the following set of equations (see Appendix D.2 for proof):

$$\mathbf{J}^{\mathrm{bd}}_{\mathrm{i},h} = -\boldsymbol{\sigma}^{\mathrm{bd}}_{\mathrm{i},h}\boldsymbol{\nabla}V_{\mathrm{i},h}, \tag{30a}$$

$$\mathbf{J}^{\mathrm{bd}}_{\mathrm{e},h} = -\boldsymbol{\sigma}^{\mathrm{bd}}_{\mathrm{e},h}\boldsymbol{\nabla}V_{\mathrm{e}}, \tag{30b}$$

$$\mathbf{J}^{\mathrm{bd}}_{\mathrm{e}} = \sum_{h=1}^{H}\alpha_h\mathbf{J}^{\mathrm{bd}}_{\mathrm{e},h}, \tag{30c}$$

$$J^{\mathrm{bd}}_{\mathrm{m},h} = C_{\mathrm{m},h}\frac{dV_{\mathrm{m,L},h}}{dt} + \frac{V_{\mathrm{m,L},h}}{R_{\mathrm{m},h}}, \tag{30d}$$

$$0 = \boldsymbol{\nabla}\cdot\mathbf{J}^{\mathrm{bd}}_{\mathrm{i},h} + \beta_h\mathbf{J}^{\mathrm{bd}}_{\mathrm{m},h}, \tag{30e}$$

$$0 = \boldsymbol{\nabla}\cdot\mathbf{J}^{\mathrm{bd}}_{\mathrm{e}} - \sum_{h=1}^{H}\alpha_h\beta_h J^{\mathrm{bd}}_{\mathrm{m},h}, \tag{30f}$$

$$\boldsymbol{\sigma}^{\mathrm{bd}}_{\mathrm{i},h} = \sigma^{\mathrm{bd}}_{\mathrm{i,L},h}\mathbf{u}_h\mathbf{u}_h^T, \tag{30g}$$

$$\boldsymbol{\sigma}^{\mathrm{bd}}_{\mathrm{e},h} = \sigma^{\mathrm{bd}}_{\mathrm{i,T},h}\mathbf{I} + (\sigma^{\mathrm{bd}}_{\mathrm{i,L},h} - \sigma^{\mathrm{bd}}_{\mathrm{i,T},h})\mathbf{u}_h\mathbf{u}_h^T, \tag{30h}$$

where, as in the fibre bundle case, $\sigma^{\rm bd}_{{\rm i,L},h} \approx 1/\rho_{{\rm i},h}$, $\sigma^{\rm bd}_{{\rm e,L},h} \approx 2d_h/b_h\rho_{\rm e}$, $\sigma^{\rm bd}_{{\rm e,T},h} \approx d_h/b_h\rho_{\rm e}$, and $\beta_h = 2/b_h$.

Solving this set of equations with finite element software can become difficult if the number of intracellular domains, H, is large (say larger than 10). In this case, a small number of domains can be used to approximate a larger number (e.g., sampling 10 discrete orientations).

4. Interpretation of Analytic Results

The cellular composite volume conductor model derived here is distinguished from standard volume conductor models due to the description of the electrical impedance properties of the tissue. Conventional volume conductor models consider the tissue to be purely resistive and usually isotropic, which leads to a constitutive equation in which the local extracellular current density is related to the instantaneous local extracellular electrical field via a simple multiplicative scalar, which is the tissue conductivity, $\mathbf{J} = -\sigma\boldsymbol{\nabla}V$. By contrast, the constitutive Equation (10a) relates the local extracellular current density to extracellular electric field via convolution in time and space with an admittivity kernel: $\mathbf{J}^{\rm vc}_{\rm e} = -\frac{1}{2\pi}\boldsymbol{\xi}^{\rm vc}_{\rm e} \underset{z,t}{*} \boldsymbol{\nabla}V_{\rm e}$. Here, the transverse component of the admittivity is given by $\hat{\hat{\xi}}^{\rm vc}_{\rm e,L} = d/\rho_{\rm e}b$ (Eq. (13c)), while the longitudinal component is given by Equation (13d)

$$\hat{\hat{\xi}}^{\rm vc}_{\rm e,L}(k_z,\omega) = \frac{1}{\rho_{\rm i}}\left(\frac{1+j\omega\tau_{\rm L}+k_z^2\lambda_{0_J}^2}{1+j\omega\tau_{\rm L}+k_z^2\lambda_{0_V}^2}\right). \tag{31}$$

This more complex form for the constitutive equation has the following physical interpretation:

(i) **Anisotropy.** The tensor form for the admittivity kernel implies that the admittivity can, in general, vary according to the direction of extracellular current flow. For a simple bundle of parallel fibres, extracellular current is more readily conducted in the longitudinal direction of fibres than the transverse direction for a given extracellular electric field strength. This can be seen by considering the ratio of the longitudinal and transverse components of the admittivity above. For more general situations, in which neurites cross, the relative admittivities in different directions will depend on the particular arrangement of neurites. While anisotropy is not a particularly novel aspect of volume conductor models, the quantitative relationship between the degree of anisotropy and the underlying microstructure of the tissue, given here, is novel.

(ii) **Finite Memory.** The convolution in time in Equation (10a) means that the local extracellular current density is related to the extracellular electric field at previous points in time (as well as the instantaneous electric field). This is due to the membrane capacitance of surrounding neural tissue, which stores charge that is released as a capacitive current at later times. For electrical pulses in excess of a

micro-second duration, as typically used in neural stimulation, this occurs through membrane charging of the longitudinal mode (the time constant associated with the transverse modes are sub-microsecond). Such charging and discharging is related to the membrane time constant, τ_{L}, via the $\omega\tau_{\mathrm{L}}$ terms in Equation (31) and can last up to a few milliseconds to reach equilibrium. The capacitive properties of tissue have been modelled previously using volume conductors, but again without relating this to the underlying microstructure of the tissue accurately [41].

(iii) **Non-locality.** The convolution in space in Equation (10a), in the longitudinal direction(s), is the most novel and unusual aspect of the volume conductor model derived here. It implies that the local current density depends on the electric field at remote longitudinal locations and not just the local electric field. The explanation for this non-local behaviour is that the spatial convolution takes into account the passage of current between points in the extracellular space via intracellular pathways along a neurite. The passage of current through the intracellular space has the effect of increasing the effective conductivity in the longitudinal direction(s) compared to the transverse direction(s). This effect is only pronounced at spatial frequencies with wavelengths that are comparable or longer than the effective electrotonic length constants ($\lambda_{\mathrm{V}}(\omega)$ and $\lambda_{\mathrm{J}}(\omega)$, see Table 2.2); for example, when the stimulating electrode is separated from the fibre by a distance comparable to the effective electronic length constants or longer ($|\lambda_{\mathrm{J}}(\omega)|$ varies between 10 and 1000 μm depending of the dominant temporal frequency of stimulation). The relationship to the electrotonic length constants arises because the extracellular current can only access the intracellular space over distances determined by electrotonic length constants. For relatively high spatial frequencies (e.g., close to the electrode), the current is forced to pass through the confined extracellular space, which leads to a relatively low effective conductivity, comparable to the transverse conductivity.

The combination of these effects gives rise to non-trivial spatio-temporal filtering of the electrical stimulation by the tissue. In the companion paper [42], these effects have been illustrated in comparison to standard volume conductor models in the case of a point source in an extensive fibre bundle.

4.1. Limiting Cases

These effects can be further understood by considering the admittivity given in Equation (31) in the following limits: far field, near field, long time, short time.

In the far field limit, where $k_z\lambda_{0_J} < k_z\lambda_{0_V} \ll 1$ and $\hat{\tilde{\xi}}^{\mathrm{vc}}_{\mathrm{e,L}}(k_z,\omega) \to 1/\rho_{\mathrm{i}}$ in Equation (31), the volume conductor model becomes an anisotropic volume conductor with simple resistive properties (i.e., no capacitive or non-local effects). Physically, this means that, in the far field, where the spatial scales at which the extracellular potential varies are large compared to the electronic length constant (for voltage), most current can enter the low impedance intracellular pathway via the membrane giving an effective

resistivity ρ_{i} in the longitudinal direction. The resistivity in the transverse direction remains at the relatively high value of $b\rho_{\mathrm{e}}/d$.

This same limit of a simple resistive anisotropic conductivity can also be obtained by using very short pulses/high temporal frequencies (i.e., $\omega\tau_{\mathrm{m}} \to \infty$ in Equation (31)) for which the membrane acts in a purely capacitive manner with negligible impedance (capacitive admittance is proportional to temporal frequency).

In general, there is a co-dependence between the temporal frequency and spatial frequencies at which the longitudinal impeditivity is well approximated by the intracellular resistivity:

$$\frac{k_z^2\lambda_{0_{\mathrm{V}}}^2}{|1+j\omega\tau_{\mathrm{L}}|} \equiv k_z^2|\lambda_{\mathrm{V}}^2(\omega)| \ll 1. \tag{32}$$

This can be derived from Equation (31) by dividing numerator and denominator by $1+j\omega\tau_{\mathrm{L}}$ and noting that it is sufficient for $k_z^2|\lambda_{\mathrm{V}}^2(\omega)| \ll 1$ since $\lambda_{\mathrm{J}}^2(\omega) < \lambda_{\mathrm{V}}^2(\omega)$. Note here that the inequality does not relate ω directly to the membrane time constant, τ_{L}; rather $\omega\tau_{\mathrm{L}}$ may need to be either greater than one or less than one, depending on the value of $k_z^2\lambda_{0_{\mathrm{V}}}^2$. The inequality can also be interpreted as a condition that the spatial frequencies are low compared to the ω-dependent electronic length constant $\lambda_{\mathrm{V}}^2(\omega)$ (for voltage).

In the limit of combined high spatial frequency, $k_z\lambda_{0_{\mathrm{V}}} > k_z\lambda_{0_{\mathrm{J}}} \gg 1$, and low temporal frequency, $\omega\tau_{\mathrm{L}}$, the longitudinal resistivity becomes $2\rho_{\mathrm{e}}d/b$, which corresponds to passage of current through the extracellular space alone. This corresponds roughly to a near field, long pulse duration limit, but the correspondence can be inexact since low as well as high spatial frequencies can exist in the near field for large electrodes [42]. In this limit, the resistivity in the longitudinal and transverse directions differs by only a factor of two ($2\rho_{\mathrm{e}}d/b$ vs. $\rho_{\mathrm{e}}d/b$, respectively), which is much closer to being isotropic than the far field case.

Summarising this discussion on limits: in the vicinity of a small electrode for long pulse durations, neural tissue is effectively more highly resistive compared to large distances or short pulse durations. In the case that some anisotropy exits due to neurites having a preferred orientation, tissue appears more isotropic near the electrode with long pulse durations than it does either far from the electrode or with short pulse durations. This has a gross effect on the current flow and the distribution of the extracellular potential that is not captured by conventional volume conductor models.

4.2. Interpretation of Extracellular Current Densities

While the quantities V_{e}, V_{i} and V_{m} are the same regardless of whether the cellular composite volume conductor or the bidomain models are used to calculate them, this is not true for the current densities in these two models. Three different equations for the extracellular current density have been given in this paper: Equation (1) for $\mathbf{\Gamma}_{\mathrm{e}}$ in the underlying model, Equation (10) for $\mathbf{J}_{\mathrm{e}}^{\mathrm{vc}}$ in the cellular composite volume conductor model and Equation (19b) for $\mathbf{J}_{\mathrm{e}}^{\mathrm{bd}}$ in the bidomain model. How are these

different current densities related? The "true" current density is of course $\mathbf{\Gamma}_\mathrm{e}$. This is not generally equal to $\mathbf{J}_\mathrm{e}^\mathrm{vc}$ except on the boundaries of NTES elements where the component of these two current densities normal to the NTES surface are approximately equal (by construction) for the longitudinal, $n = 0$, and the transverse, $n = 1$, modes of stimulation. Beyond the NTES boundary, much of the $\mathbf{\Gamma}_\mathrm{e}$ current will be forced through the confined extracellular space of conductivity ρ_e^{-1}, while the $\mathbf{J}_\mathrm{e}^\mathrm{vc}$ current is free to pass through the whole volume previously occupied by the NTES, which has been replaced by a homogeneous volume conductor with admittivity kernel $\boldsymbol{\xi}_\mathrm{e}^\mathrm{vc}$. This can be visualised by comparing Figures 3(a) and 3(b). Due to this constriction,the directions of $\mathbf{\Gamma}_\mathrm{e}$ and $\mathbf{J}_\mathrm{e}^\mathrm{vc}$ will generally be different, and the magnitude of $\mathbf{\Gamma}_\mathrm{e}$ will be generally higher than the magnitude of $\mathbf{J}_\mathrm{e}^\mathrm{vc}$ at any (infinitely small) point in the extracellular space. However, when these two current densities are averaged over an area comparable to the diameter of a neurite or larger, they will be approximately equal in both longitudinal and transverse directions. The extracellular current densities for the cellular composite bidomain and volume conductor models are equal in the transverse direction $\mathbf{J}_\mathrm{e,T}^\mathrm{bd} = \mathbf{J}_\mathrm{e,T}^\mathrm{vc}$ only. In the longitudinal direction, the situation is more complicated: the change in the longitudinal current densities in the longitudinal direction is different by an amount proportional to the membrane current density: $\frac{dJ_\mathrm{e,L}^\mathrm{bd}}{dz} = \frac{dJ_\mathrm{e,L}^\mathrm{vc}}{dz} + \beta J_\mathrm{m}$.

5. Discussion

5.1. Limitations of the current work

Several approximations have been used in the modelling framework derived here. These are discussed below.

- $d \ll b$: that the width of the extracellular space is much less than the radius of neurites. Although b is strictly the radius of the neurite plus the thin extracellular sheath, $(b = a + d)$, we have taken b to be synonymous with the neurites actual radius throughout, which is consistent with the approximation. The approximation is justified due to the extremely confined nature of the extracellular space relative to the intracellular space, so that $d/b < 1/10$ generally. The approximation is used to both derive and simplify the expressions for the neurite equation and transimpedance equations.
- $\omega\tau_{\mathrm{T_J}} < \omega\tau_{\mathrm{T_V}} \ll 1$. This condition assumes that for stimulus pulse widths used to drive electrodes, the temporal frequencies that dominate the spectrum (i.e., that have non-negligible amplitude) are much faster than the time constants for charging the neural membrane in the transverse mode. This charging is very fast, so that this approximation is good for pulse widths in excess of 1μs which are relevant to neural stimulation. The approximation allows us to simplify expressions for the transverse component of the NTES transimpedance so that it may be considered to reflect the purely resistive extracellular pathway in this direction. However, it could be relaxed if higher temporal frequencies were of interests, at the cost of more

complicated expressions. The approximation has been applied elsewhere to model transverse stimulation [31].

- The mean-field approximation used to derive the admittivity of the cellular composite volume conductor models requires a spatial averaging over scales of several neurites radii. This has two implications.
  - First, predictions of the model should be treated with caution for electrode-neurite separations that are not substantially larger than b. A similar requirement emerges in the derivation of the neurite equations, where the fluctuations in the extracellular potential and current density must occur on a scale much greater than b, see [25]. As b is typically on the order of a micron, this is not a restrictive limitation in neural prosthetic applications, in which electrodes are rarely less than 10μm from target neurons.
  - Second, the model expressions given here in the Stage 1 volume conductor are for the mean extracellular potential and tissue admittivity in small volume, but neglect effects of microscopic spatial variation. The mean is taken over different cellular types, orientations and sizes, and so, captures these effects to first order. Second order effects, due to microscopic spatial variation in these quantities, such as a constriction in an axon, are not captured at the level of Stage 1 quantities. It is feasible to address the effect of such variation at the level of the Stage 2 neurite equations, however. This can be done by applying the mean-field expression for V_e to a model of a neurite with microscale spatial variation, such as a morphologically reconstructed multicompartmental model neuron. As long as the probability distribution of the properties of the various compartments of the model neuron, such as orientation, size and membrane resistance, have been taken into account in performing the averaging of mean-field in Stage 1, the whole two-stage model will be self-consistent.

Another limitation is that the modeling framework presented here applies to the passive electrical properties of tissue and neurites only. This is required in the derivation to decompose quantities into their longitudinal and transverse components and to perform the spatial and temporal Fourier analysis. The effects of non-linear membrane properties, such as the voltage-gated ion channels underlying spike generation are neglected. This has implications for both stages of the volume conductor model. In Stage 1 of the volume conductor model, it is reasonable to argue that the time-dependent changes in membrane conductance associated with the activation of these channels become significant only once a spike has been initiated. Hence, the spatial and temporal distribution of extracellular potential or current density that lead to the spike prior to its initiation can be estimated with a passive model.

In Stage 2 of the volume conductor model, the purely passive model underscores that point that no mechanism has been specified to determine when a spike occurs. A simple choice is to specify a sigmoidal transfer function, $g(V_\mathrm{m})$ which gives the probability of a spike being initiated as a function of the passive membrane potential. A

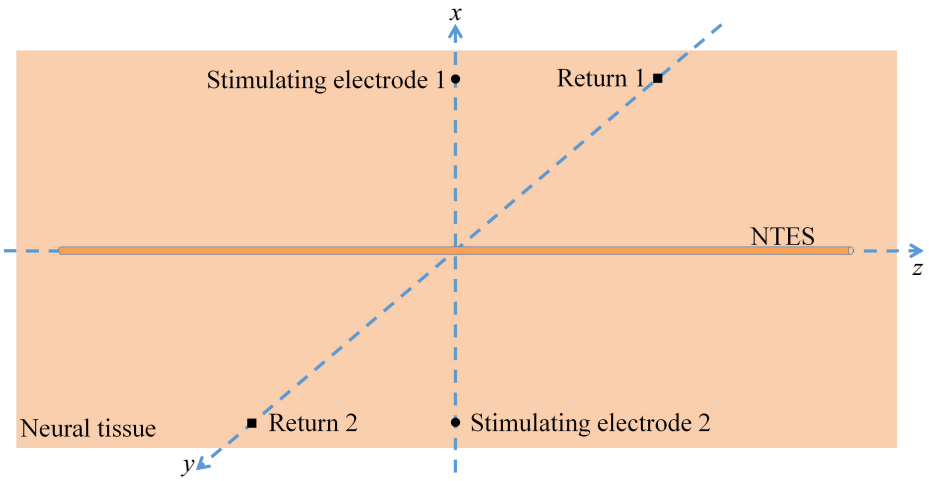

Figure 4. A neurite in neural tissue. In this configuration with two stimulating and two return electrodes, the $n = 1$ terms from the stimulating electrodes cancel each other out. The $n = 2$ term is the most significant transverse component for the neurite shown in this figure.

complication is that V_{m} varies both in time (during and after the pulse) and space (along the neurite). To contend with this, one choice is to consider only the maximum value of V_{m}, both along the neurite, and during and immediately after the pulse. However, one needs to consider that the transfer function, g, may change depending on both the position on the neurite, e.g. thresholds are lower in the Na^+ band of the axon initial segment relative to other parts of the axon [43], the pulse waveform or the mode of stimulation (longitudinal vs. transverse). A second possibility to incorporate spiking behaviour is to use a passive model in Stage 1, but apply it to a non-linear Stage 2 cable equation or multicompartmental model for the longitudinal mode, which includes Hodgkin-Huxley type dynamics. This can also be done in the bi-/multi-domain approach for the longitudinal mode.

We have shown in our previous work [27] that the effect of higher order terms ($n \geq 2$) are generally negligible and their magnitudes are proportional to $1/n^2$ in calculating the membrane potential, V_{m}, for a given extracellular potential, V_{e}. Given that in calculating V_{e}, higher order terms ($n \geq 2$) are small, the overall contribution to the membrane potential from the terms $n \geq 2$ becomes negligible. Therefore, we have not considered higher order terms in the current model. Although it is desirable to incorporate higher order terms, the model intrinsically has only two degrees of freedom due to the axial symmetry of cylindrical neurons: one along the fibers and the other across the fibers. We will investigate the effect of higher order terms and their convergence rate in our future work involving full scale finite element simulation of neural tissue.

In the case of symmetric stimulation with two stimulating electrodes and two return electrodes, as shown in Figure 4, for the neurite between the two stimulating electrodes at $r = 0$ (along the z-axis), the $n = 1$ terms cancel each other out. Therefore, the

$n = 2$ term becomes the most significant transverse component, although it is negligible compared to the longitudinal mode, $n = 0$.

5.2. Relation to previous work

Several previous studies have provided theoretical estimates of the electrical properties of tissue on the basis of their cellular composition. Several studies have considered tissue as a collection of cells sparsely suspended in an extracellular medium [15, 30, 31, 44], however this is not the situation considered here of densely packed, elongated fibres, which is characteristic of neural tissue.

One of the earliest studies to consider neural tissue as a densely packed composite of long (cable-like) processes was done by Ranck [45]. His aim was to estimate the temporal frequency dependence of the admittivity of cortical grey matter and compare it to measured values. His approach considered the admittivity to be a sum of components due to the longitudinal admittivity of neurons, glia and blood vessels, as well as the admittivity of a restricted extracellular space; he then performed an average over different fibre directions to obtain a final answer. This is similar to our approach for deriving the general cellular composite volume conductor models of Section 3.3 and especially the expression for the combined tissue admittivity, Equation(29). One major difference is that the spatial frequency dependence of the admittivity was not considered, and his estimate is essentially a mid-field estimate between near- and far-field. Another is that he did not relate his results to modelling extracellular electrical stimulation, as we do here by placing the derivation of the admittivity in the context of volume conductor and neurite stimulation models. Rather, he showed that the resulting admittivity has a temporal frequency dispersion below 5kHz, similar to his measurement of cortical gray matter, which was attributable to the capacitive effect of charging the neural membranes in the longitudinal mode. Further analysis will be required to determine if a similar result holds for the models described here.

Most previously studies of bi-domain models have considered the intracellular domain to have non-zero conductivity in multiple directions [46], whereas here any given intracellular domain has non-zero conductivity in only the longitudinal direction. In the class of models described here, intracellular conductivity in multiple directions is the result of multiple intracellular domains with different orientations. This is consistent with the notion that current cannot flow freely between different intracellular domains without crossing a membrane. Multi-domain models that account for this effect have not been considered previously.

A few bi-domain studies have used a formulation that is equivalent to the one described here in the case of a fibre bundle [40, 47, 48]. As this is the subject to the companion paper [42], this will be discussed further there.

A discussion of the implications of present results for extracellular stimulation of neural tissue will be given in the companion paper [42]. Beyond this, the present results may have implications in other fields of study concerned with the electrical

properties of tissue such as estimation, analysis and interpretation or recorded intrinsic electrical signals in the brain such as: multi-unit activity, local field potentials and the electroencephalogram [49, 50]; electrical impedance tomography [35]; and electromagnetic dosimetry [51].

6. Conclusion

This paper develops a modelling framework for electrical stimulation of neural tissue taking account of its cellular composition. The mean-field volume conductor model, described in Sections 3.1 and 3.3, provides a basis for calculating the intracellular, extracellular and subthreshold membrane potential in a neurite under stimulation by a set of electrodes. The equations may be solved for simple tissue geometries using Fourier techniques, such as the case of spatially extensive fibre bundles (Section 3.1) or more generally collections of fibres of mixed orientation (Section 3.3). Alternatively, the bidomain/multidomain model described in Sections 3.2 and 3.3 is a mathematically equivalent way to calculate the same quantities, which is suited to implementation using commercially available finite element software packages such as ANSYS or COMSOL. This is suitable for problems with more complex tissue geometries.

The modeling framework provides a number of advantages over other approaches currently adopted in the literature.

(i) **Capturing the cellular composition of tissue in the admittivity**: The admittivity introduced here captures electrical properties of the cellular composition of densely packed neural tissue including geometric properties of the cells. This includes the effect of the confined extracellular space, the high impedance, capacitive properties of the membrane and low resistance intracellular pathway in the direction of the neurite. This has some important effects on the spatio-temporal distribution of potential and current density in the tissue that are not captured by standard models.

(ii) **Self-consistent modelling of membrane potential**: The approach allows self-consistent calculation of the membrane potential using a two-stage volume conductor model, independent of whether current- or voltage-type boundary conditions are used in Stage 2. By contrast, standard two-stage volume conductor models treat the tissue admittivity simplistically and give internally inconsistent results.

(iii) **Computational efficiency**: The modelling framework described here has a similar computational burden to standard two-stage volume conductor models or bidomain models. By contrast, full scale modelling of a composite of closely packed neurites rapidly becomes computationally intractable.

(iv) **Equivalent multidomain models**: For every self-consistent volume conductor model, we have given a mathematically equivalent multidomain model. This provides a mathematically rigorous connection between the two model types and

the common underlying cellular geometry of the tissue.

(v) **Calculation of longitudinal and transverse modes**: Both transverse and longitudinal modes of the subthreshold membrane can be calculated and compared within a unified framework.

7. Acknowledgements

This research was supported by the Australian Research Council (ARC) through its Special Research Initiative (SRI) in Bionic Vision Science and Technology grant to Bionic Vision Australia (BVA). The Bionics Institute acknowledges the support it receives from the Victorian Government through its Operational Infrastructure Support Program. This research was supported by a Victorian Life Sciences Computation Initiative (VLSCI) grant number VR0138 on its Peak Computing Facility at the University of Melbourne, an initiative of the Victorian Government.

Appendix A. Calculations for Extracellular Voltage and Current Density in Volume Conductor Model

For steady state currents, the equation of continuity may be written as

$$\boldsymbol{\nabla} \cdot \mathbf{J}_{\mathrm{e}} = \frac{\partial J_{\mathrm{e},x}}{\partial x} + \frac{\partial J_{\mathrm{e},y}}{\partial y} + \frac{\partial J_{\mathrm{e},z}}{\partial z} = 0. \tag{A.1}$$

where $J_{\mathrm{e},x}$, $J_{\mathrm{e},y}$, and $J_{\mathrm{e},z}$ are the components of the current density in tissue. Consider the coordinate setup shown in Figure Appendix A with a neurite centred at point (x, y) in the xy-plane. Using Taylor series expansion, the extracellular voltage, V_{e}, at the boundary of the neurite is calculated to be

$$V_{\mathrm{e}}(\tilde{x} = x + b\cos\theta, \tilde{y} = y + b\sin\theta, \tilde{z} = z) = V_{\mathrm{e}}(x, y, z) + b\cos\theta\ \frac{\partial V_{\mathrm{e}}}{\partial x} + b\sin\theta\ \frac{\partial V_{\mathrm{e}}}{\partial y} + \mathcal{O}(b^2). \tag{A.2}$$

Therefore, the extracellular potential in the Fourier θ-transform domain can be written as

$$\bar{V}_{\mathrm{e}}[\tilde{x}, \tilde{y}](z, n, t) = \frac{1}{2\pi} \int_{2\pi} \left(V_{\mathrm{e}}(x, y, z, t) + b\cos\theta \frac{\partial V_{\mathrm{e}}(x, y, z, t)}{\partial x} + b\sin\theta \frac{\partial V_{\mathrm{e}}(x, y, z, t)}{\partial y} \right) e^{-jn\theta} d\theta, \tag{A.3}$$

thus,

$$\bar{V}_{\mathrm{e}}[\tilde{x}, \tilde{y}](z, 0, t) = V_{\mathrm{e}}(x, y, z, t), \tag{A.4a}$$

$$\bar{V}_{\mathrm{e}}[\tilde{x}, \tilde{y}](z, 1, t) = \frac{b}{2} \left(\frac{\partial V_{\mathrm{e}}(x, y, z, t)}{\partial x} - j \frac{\partial V_{\mathrm{e}}(x, y, z, t)}{\partial y} \right). \tag{A.4b}$$

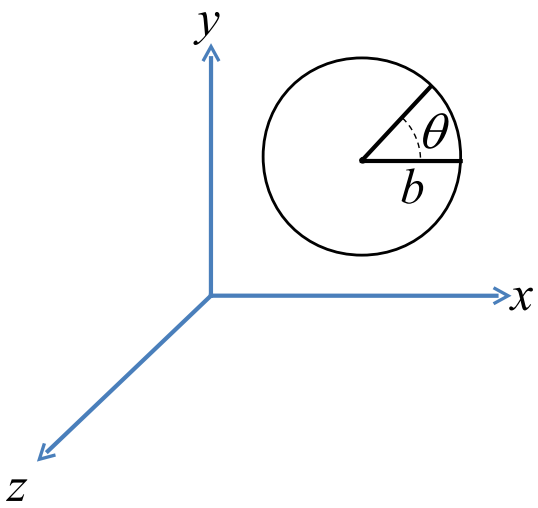

Figure A1. A neurite in tissue.

Using Taylor series expansion for current density leads to

$$J_{\mathrm{e},x}(\tilde{x}{=}x{+}b\cos\theta,\tilde{y}{=}y{+}b\sin\theta,z,t){=}J_{\mathrm{e},x}(x,y,z,t){+}b\cos\theta\,\frac{\partial J_{\mathrm{e},x}}{\partial x}{+}b\sin\theta\,\frac{\partial J_{\mathrm{e},x}}{\partial y}{+}\mathcal{O}(b^2), \tag{A.5a}$$

$$J_{\mathrm{e},y}(\tilde{x}{=}x{+}b\cos\theta,\tilde{y}{=}y{+}b\sin\theta,z,t){=}J_{\mathrm{e},y}(x,y,z,t){+}b\cos\theta\,\frac{\partial J_{\mathrm{e},y}}{\partial x}{+}b\sin\theta\,\frac{\partial J_{\mathrm{e},y}}{\partial y}{+}\mathcal{O}(b^2), \tag{A.5b}$$

Taking into account that in the xy-plane

$$\begin{aligned}\mathbf{J}_{\mathrm{e}}[\tilde{x},\tilde{y}](z,\theta,t)\cdot\mathbf{n} &= [J_{\mathrm{e},x}(\tilde{x},\tilde{y},z,t)\;\; J_{\mathrm{e},y}(\tilde{x},\tilde{y},z,t)]\begin{bmatrix}\cos\theta\\ \sin\theta\end{bmatrix}\\ &= J_{\mathrm{e},x}(x,y,z,t)\cos\theta + J_{\mathrm{e},y}(x,y,z,t)\sin\theta + b\cos^2\theta\,\frac{\partial J_{\mathrm{e},x}}{\partial x}\\ &\quad + b\cos\theta\sin\theta\,\frac{\partial J_{\mathrm{e},x}}{\partial y} + b\sin\theta\cos\theta\,\frac{\partial J_{\mathrm{e},y}}{\partial x} + b\sin^2\theta\,\frac{\partial J_{\mathrm{e},y}}{\partial y},\end{aligned} \tag{A.6}$$

we calculate

$$\bar{\mathbf{J}}_{\mathrm{e}}[\tilde{x},\tilde{y}](z,n,t)\cdot\mathbf{n} = \frac{1}{2\pi}\int_{2\pi}\mathbf{J}_{\mathrm{e}}[\tilde{x},\tilde{y}](z,\theta,t)\cdot\mathbf{n}\;e^{-jn\theta}d\theta, \tag{A.7}$$

therefore,

$$\bar{\mathbf{J}}_{\mathrm{e}}[\tilde{x},\tilde{y}](z,0,t)\cdot\mathbf{n} = \frac{b}{2}\left(\frac{\partial J_{\mathrm{e},x}(x,y,z,t)}{\partial x}+\frac{\partial J_{\mathrm{e},y}(x,y,z,t)}{\partial y}\right) = -\frac{b}{2}\frac{\partial J_{\mathrm{e},z}(x,y,z,t)}{\partial z}, \tag{A.8a}$$

$$\bar{\mathbf{J}}_{\mathrm{e}}[\tilde{x},\tilde{y}](z,1,t)\cdot\mathbf{n} = \frac{1}{2}\Big(J_{\mathrm{e},x}(x,y,z,t) - jJ_{\mathrm{e},y}(x,y,z,t)\Big). \tag{A.8b}$$

Appendix B. Derivation of the Constitutive Equation

Equations (9) in (k_z, ω) domain will be written as

$$\hat{\tilde{V}}_{\mathrm{e}}[\tilde{x},\tilde{y}](k_z,0,\omega) = \hat{V}_{\mathrm{e}}(x,y,k_z,\omega), \tag{B.1a}$$

$$\hat{\tilde{\mathbf{J}}}_{\mathrm{e}}^{\mathrm{vc}}\cdot\mathbf{n}[\tilde{x},\tilde{y}](k_z,0,\omega) = -jk_z\frac{b}{2}\hat{J}_{\mathrm{e},z}(x,y,k_z,\omega), \tag{B.1b}$$

$$\hat{\tilde{V}}_{\mathrm{e}}[\tilde{x},\tilde{y}](k_z,1,\omega) = \frac{b}{2}\left(\frac{\partial\hat{V}_{\mathrm{e}}(x,y,k_z,\omega)}{\partial x} - j\frac{\partial\hat{V}_{\mathrm{e}}(x,y,k_z,\omega)}{\partial y}\right), \tag{B.1c}$$

$$\hat{\tilde{\mathbf{J}}}_{\mathrm{e}}^{\mathrm{vc}}\cdot\mathbf{n}[\tilde{x},\tilde{y}](k_z,1,\omega) = \frac{1}{2}\Big(\hat{J}_{\mathrm{e},x}(x,y,k_z,\omega) - j\hat{J}_{\mathrm{e},y}(x,y,k_z,\omega)\Big). \tag{B.1d}$$

Using the transimpedance equation, we may express the extracellular current density, $\hat{\mathbf{J}}_{\mathrm{e}}$, in Fourier domain in terms of the extracellular voltage in Fourier domain, $\hat{V}_{\mathrm{e}}$, as follows

$$\begin{aligned}
\hat{\mathbf{J}}_{\mathrm{e}}^{\mathrm{vc}} \equiv \begin{bmatrix} \hat{J}_{\mathrm{e},x}^{\mathrm{vc}}(x,y,k_z,\omega) \\ \hat{J}_{\mathrm{e},y}^{\mathrm{vc}}(x,y,k_z,\omega) \\ \hat{J}_{\mathrm{e},z}^{\mathrm{vc}}(x,y,k_z,\omega) \end{bmatrix} &= \begin{bmatrix} -\dfrac{b}{\hat{\tilde{Z}}_{\mathrm{e}}(k_z,1,\omega)}\dfrac{\partial\hat{V}_{\mathrm{e}}(x,y,k_z,\omega)}{\partial x} \\ -\dfrac{b}{\hat{\tilde{Z}}_{\mathrm{e}}(k_z,1,\omega)}\dfrac{\partial\hat{V}_{\mathrm{e}}(x,y,k_z,\omega)}{\partial y} \\ \dfrac{2}{jk_zb\hat{\tilde{Z}}_{\mathrm{e}}(k_z,0,\omega)}\hat{V}_{\mathrm{e}}(x,y,k_z,\omega) \end{bmatrix} \\
&= \begin{bmatrix} -\dfrac{b}{\hat{\tilde{Z}}_{\mathrm{e}}(k_z,1,\omega)} & 0 & 0 \\ 0 & -\dfrac{b}{\hat{\tilde{Z}}_{\mathrm{e}}(k_z,1,\omega)} & 0 \\ 0 & 0 & \dfrac{-2j}{k_zb\hat{\tilde{Z}}_{\mathrm{e}}(k_z,0,\omega)} \end{bmatrix} \begin{bmatrix} \dfrac{\partial\hat{V}_{\mathrm{e}}(x,y,k_z,\omega)}{\partial x} \\ \dfrac{\partial\hat{V}_{\mathrm{e}}(x,y,k_z,\omega)}{\partial y} \\ \hat{V}_{\mathrm{e}}(x,y,k_z,\omega) \end{bmatrix} \\
&= -\begin{bmatrix} \dfrac{b}{\hat{\tilde{Z}}_{\mathrm{e}}(k_z,1,\omega)} & 0 & 0 \\ 0 & \dfrac{b}{\hat{\tilde{Z}}_{\mathrm{e}}(k_z,1,\omega)} & 0 \\ 0 & 0 & \dfrac{(r_{\mathrm{e}}+r_{\mathrm{i}})\Big(1+k_z^2\lambda_{\mathrm{J}}^2(\omega)\Big)}{\pi br_{\mathrm{e}}r_{\mathrm{i}}\Big(1+k_z^2\lambda_{\mathrm{V}}^2(\omega)\Big)} \end{bmatrix} \begin{bmatrix} \dfrac{\partial\hat{V}_{\mathrm{e}}(x,y,k_z,\omega)}{\partial x} \\ \dfrac{\partial\hat{V}_{\mathrm{e}}(x,y,k_z,\omega)}{\partial y} \\ jk_z\hat{V}_{\mathrm{e}}(x,y,k_z,\omega) \end{bmatrix} \\
&= -\hat{\boldsymbol{\xi}}_{\mathrm{e}}^{\mathrm{vc}}(k_z,\omega)\check{\boldsymbol{\nabla}}\hat{V}_{\mathrm{e}}(x,y,k_z,\omega),
\end{aligned} \tag{B.2}$$

where $\check{\boldsymbol{\nabla}} \triangleq [\partial/\partial x, \partial/\partial y, jk_z]$ and $\hat{\boldsymbol{\xi}}_{\mathrm{e}}^{\mathrm{vc}}(k_z,\omega)$ is the admittivity tensor in the time and space Fourier domain

$$\hat{\boldsymbol{\xi}}_{\mathrm{e}}^{\mathrm{vc}}(k_z,\omega) = \begin{bmatrix} \hat{\xi}_{\mathrm{e,T}}^{\mathrm{vc}}(k_z,\omega) & 0 & 0 \\ 0 & \hat{\xi}_{\mathrm{e,T}}^{\mathrm{vc}}(k_z,\omega) & 0 \\ 0 & 0 & \hat{\xi}_{\mathrm{e,L}}^{\mathrm{vc}}(k_z,\omega) \end{bmatrix}, \tag{B.3}$$

and, therefore,

$$\hat{\tilde{\xi}}^{\rm vc}_{\rm e,T}(k_z,\omega)=\frac{b}{\hat{\tilde{Z}}(k_z,1,\omega)}=\frac{b\Big(Z_{\rm m}(\omega)+R_{{\rm e},J}(1)+R_{{\rm i},J}(1)\Big)}{R_{{\rm e},J}(n)\Big(Z_{\rm m}(\omega)+R_{{\rm i},V}(1)+R_{{\rm e},V}(1)\Big)}\approx\frac{b}{R_{{\rm e},J}(n)}=\frac{d}{b\rho_{\rm e}},\tag{B.4a}$$

$$\hat{\tilde{\xi}}^{\rm vc}_{\rm e,L}(k_z,\omega)=\frac{(r_{\rm e}+r_{\rm i})\Big(1+k_z^2\lambda_{\rm J}^2(\omega)\Big)}{\pi b r_{\rm e} r_{\rm i}\Big(1+k_z^2\lambda_{\rm V}^2(\omega)\Big)}\approx\frac{1}{\rho_{\rm i}}\frac{\Big(1+k_z^2\lambda_{\rm J}^2(\omega)\Big)}{\Big(1+k_z^2\lambda_{\rm V}^2(\omega)\Big)}.\tag{B.4b}$$

Equation (B.2) can be transformed into (z,ω) domain by applying an inverse Fourier transform in terms of k_z which results in

$$\hat{\mathbf{J}}^{\rm vc}_{\rm e}(x,y,z,\omega)=-\frac{1}{\sqrt{2\pi}}\hat{\boldsymbol{\xi}}^{\rm vc}(z,\omega)\underset{z}{*}\boldsymbol{\nabla}\hat{V}_{\rm e}(x,y,z,\omega).\tag{B.5}$$

Applying inverse Fourier time-transform to the Equation (B.5) leads to

$$\mathbf{J}^{\rm vc}_{\rm e}(x,y,z,t)=-\frac{1}{2\pi}\boldsymbol{\xi}^{\rm vc}(z,t)\underset{z,t}{*}\boldsymbol{\nabla}V_{\rm e}(x,y,z,t).\tag{B.6}$$

Appendix C. Representations of the Volume Conductor Model

Tables C1 and C2 give the complete volume conductor model as well as membrane potential equations in four different representations: (k_z,ω), (z,ω), (k_z,t) and (z,t) domains. In these tables, we have presented differential equations to calculate $V^{\rm Max}_{\rm m,T}$, the maximum value of the transverse component over all possible values of θ which is desirable in electrical stimulation. If one is interested in calculating $V_{\rm m,T}$ for all θ then $V_{\rm m,T}$ should be treated as a complex number. For example, the transverse equation for current density boundary condition in (z,t) domain should be written as

$$\left(\tau_{\rm T,J}\frac{dV_{\rm m,T}}{dt}+V_{\rm m,T}\right)(\cos\theta+j\sin\theta)=-\frac{R_{\rm m}R_{{\rm e},J}(1)}{2(R_{\rm m}+R_{{\rm i},J}(1)+R_{{\rm e},J}(1))}(J_{{\rm e},x}-jJ_{{\rm e},y}),\tag{C.1}$$

and therefore, two differential equations for real and imaginary parts should be solved.

Table C1. Equations for volume conductor model in various coordinates.

Equation	(k_z, ω)	(z, ω)
Constitutive Eq.	$\hat{\tilde{\mathbf{J}}}_{\mathrm{e}} = \hat{\tilde{\boldsymbol{\xi}}}_{\mathrm{e}}^{\mathrm{vc}} \check{\boldsymbol{\nabla}} \hat{\tilde{V}}_{\mathrm{e}}$	$\hat{\mathbf{J}}_{\mathrm{e}} = \hat{\boldsymbol{\xi}}_{\mathrm{e}}^{\mathrm{vc}} \underset{z}{*} \boldsymbol{\nabla} \hat{V}_{\mathrm{e}}$
Continuity Eq.	$\check{\boldsymbol{\nabla}} \cdot \hat{\tilde{\mathbf{J}}}_{\mathrm{e}} = \mathbf{0}$	$\boldsymbol{\nabla} \cdot \hat{\mathbf{J}}_{\mathrm{e}} = \mathbf{0}$
Conductivity		
Longitudinal	$\hat{\tilde{\xi}}_{\mathrm{e,L}}^{\mathrm{vc}} = \frac{1}{\rho_{\mathrm{i}}} \frac{1 + k_z^2 \lambda_{\mathrm{J}}^2(\omega)}{1 + k_z^2 \lambda_{\mathrm{V}}^2(\omega)}$	$\hat{\xi}_{\mathrm{e,L}}^{\mathrm{vc}} = \frac{2d\sqrt{2\pi}}{b\rho_{\mathrm{e}}} \delta(z) + \sqrt{\frac{\pi}{2}} \frac{1}{\rho_{\mathrm{i}} \lambda_{\mathrm{V}}(\omega)} \exp\left(-\frac{\lvert z \rvert}{\lambda_{\mathrm{V}}(\omega)}\right)$
Transverse	$\hat{\tilde{\xi}}_{\mathrm{e,T}}^{\mathrm{vc}} = \frac{d}{\rho_{\mathrm{e}} b}$	$\hat{\xi}_{\mathrm{e,T}}^{\mathrm{vc}} = \frac{d}{\rho_{\mathrm{e}} b} \sqrt{2\pi} \delta(z)$
Membrane Eq. Voltage BC		
Longitudinal	$\hat{\tilde{V}}_{\mathrm{m,L}} = -\frac{k_z^2 \lambda_{\mathrm{V}}^2(\omega)}{1 + k_z^2 \lambda_{\mathrm{V}}^2(\omega)} \hat{\tilde{V}}_{\mathrm{e}}$	$\lambda_{\mathrm{V}}^2(\omega) \frac{\partial^2 \hat{V}_{\mathrm{m,L}}}{\partial z^2} - \hat{V}_{\mathrm{m,L}} = -\lambda_{\mathrm{V}}^2(\omega) \frac{\partial^2 \hat{V}_{\mathrm{e}}}{\partial z^2}$
Transverse	$\hat{\tilde{V}}_{\mathrm{m,T}}^{\mathrm{Max}} = -\frac{Z_{\mathrm{m}}}{(Z_{\mathrm{m}} + R_{\mathrm{i,V}}(1) + R_{\mathrm{e,V}}(1))} \hat{\tilde{V}}_{\mathrm{e,T}}$	$\hat{V}_{\mathrm{m,T}}^{\mathrm{Max}} = -\frac{Z_{\mathrm{m}}}{(Z_{\mathrm{m}} + R_{\mathrm{i,V}}(1) + R_{\mathrm{e,V}}(1))} \hat{V}_{\mathrm{e,T}}$
Membrane Eq. Current BC		
Longitudinal	$\hat{\tilde{V}}_{\mathrm{m,L}} = -\frac{j k_z \lambda_{\mathrm{J}}^2(\omega)}{1 + k_z^2 \lambda_{\mathrm{J}}^2(\omega)} \frac{b\rho_{\mathrm{e}}}{2d} \hat{\tilde{J}}_{\mathrm{e},z}$	$\lambda_{\mathrm{J}}^2(\omega) \frac{\partial^2 \hat{V}_{\mathrm{m,L}}}{\partial z^2} - \hat{V}_{\mathrm{m,L}} = \lambda_{\mathrm{J}}^2(\omega) \frac{\rho_{\mathrm{e}} b}{2d} \frac{\partial \hat{J}_{\mathrm{e},z}}{\partial z}$
Transverse	$\hat{\tilde{V}}_{\mathrm{m,T}}^{\mathrm{Max}} = \frac{Z_{\mathrm{m}} R_{\mathrm{e,J}}(1)}{(Z_{\mathrm{m}} + R_{\mathrm{i,J}}(1) + R_{\mathrm{e,J}}(1))} \hat{\tilde{J}}_{\mathrm{e,T}}$	$\hat{V}_{\mathrm{m,T}}^{\mathrm{Max}} = \frac{Z_{\mathrm{m}} R_{\mathrm{e,J}}(1)}{(Z_{\mathrm{m}} + R_{\mathrm{i,J}}(1) + R_{\mathrm{e,J}}(1))} \hat{J}_{\mathrm{e,T}}$

Table C2. Equations for volume conductor model in various coordinates.

Equation	(k_z, t)	(z, t)
Constitutive Eq.	$\check{\mathbf{J}}_{\mathrm{e}} = \check{\boldsymbol{\xi}}_{\mathrm{e}}^{\mathrm{vc}} \underset{t}{*} \check{\boldsymbol{\nabla}} \check{V}_{\mathrm{e}}$	$\mathbf{J}_{\mathrm{e}} = \boldsymbol{\xi}_{\mathrm{e}}^{\mathrm{vc}} \underset{z,t}{*} \boldsymbol{\nabla} V_{\mathrm{e}}$
Continuity Eq.	$\check{\boldsymbol{\nabla}} \cdot \check{\mathbf{J}}_{\mathrm{e}} = \mathbf{0}$	$\boldsymbol{\nabla} \cdot \mathbf{J}_{\mathrm{e}} = \mathbf{0}$
Conductivity		
Longitudinal	$\check{\xi}_{\mathrm{e,L}}^{\mathrm{vc}} = \frac{\sqrt{2\pi}}{\rho_{\mathrm{i}}}\delta(t) - \frac{k_z^2 \lambda_{0_{\mathrm{V}}}^2 \sqrt{2\pi} H(t)}{\rho_{\mathrm{i}} \tau_{\mathrm{m}}} e^{-(1+k_z^2\lambda_{0_{\mathrm{V}}}^2)\frac{t}{\tau_{\mathrm{m}}}}$	$\xi_{\mathrm{e,L}}^{\mathrm{vc}} = \frac{2\pi\delta(z)\delta(t)}{\rho_{\mathrm{i}}} - \frac{\sqrt{\pi} H(t) \tau_{\mathrm{m}}^{\frac{3}{2}}}{4\rho_{\mathrm{i}}\lambda_{0_{\mathrm{V}}} t^{\frac{5}{2}}} \left(\frac{2t}{\tau_{\mathrm{m}}} - \frac{z^2}{\lambda_{0_{\mathrm{V}}}^2}\right) e^{-\left(\frac{t}{\tau_{\mathrm{m}}} + \frac{z^2}{4\lambda_{0_{\mathrm{V}}}^2}\frac{\tau_{\mathrm{m}}}{t}\right)}$
Transverse	$\check{\xi}_{\mathrm{e,T}}^{\mathrm{vc}} = \frac{d}{\rho_{\mathrm{e}} b}\sqrt{2\pi}\delta(t)$	$\xi_{\mathrm{e,T}}^{\mathrm{vc}} = \frac{d}{\rho_{\mathrm{e}} b} 2\pi\delta(z)\delta(t)$
Membrane Eq. Voltage BC		
Longitudinal	$\frac{\tau_{\mathrm{L}}}{1+k_z^2\lambda_{0_{\mathrm{V}}}^2}\frac{d\check{V}_{\mathrm{m,L}}}{dt} + \check{V}_{\mathrm{m,L}} = -\frac{k_z^2\lambda_{0_{\mathrm{V}}}^2}{1+k_z^2\lambda_{0_{\mathrm{V}}}^2}\check{V}_{\mathrm{e}}$	$\lambda_{0_{\mathrm{V}}}^2 \frac{\partial^2 V_{\mathrm{m,L}}}{\partial z^2} - \tau_{\mathrm{L}}\frac{\partial V_{\mathrm{m,L}}}{\partial t} - V_{\mathrm{m,L}} = -\lambda_{0_{\mathrm{V}}}^2 \frac{\partial^2 V_{\mathrm{e}}}{\partial z^2}$
Transverse	$\tau_{\mathrm{T_V}}\frac{d\check{V}_{\mathrm{m,T}}^{\mathrm{Max}}}{dt} + \check{V}_{\mathrm{m,T}}^{\mathrm{Max}} = -\frac{R_{\mathrm{m}}}{(R_{\mathrm{m}} + R_{\mathrm{i,V}}(1) + R_{\mathrm{e,V}}(1))}\check{V}_{\mathrm{e,T}}$	$\tau_{\mathrm{T_V}}\frac{d\lvert V_{\mathrm{m,T}}\rvert}{dt} + \lvert V_{\mathrm{m,T}}\rvert = -\frac{R_{\mathrm{m}}}{(R_{\mathrm{m}} + R_{\mathrm{i,V}}(1) + R_{\mathrm{e,V}}(1))} V_{\mathrm{e,T}}$
Membrane Eq. Current BC		
Longitudinal	$\frac{\tau_{\mathrm{L}}}{1+k_z^2\lambda_{0_{\mathrm{J}}}^2}\frac{d\check{V}_{\mathrm{m,L}}}{dt} + \check{V}_{\mathrm{m,L}} = \frac{jk_z\lambda_{0_{\mathrm{J}}}^2}{1+k_z^2\lambda_{0_{\mathrm{J}}}^2}\frac{b\rho_{\mathrm{e}}}{2d}\check{J}_{\mathrm{e},z}$	$\lambda_{0_{\mathrm{J}}}^2 \frac{\partial^2 V_{\mathrm{m,L}}}{\partial z^2} - \tau_{\mathrm{L}}\frac{\partial V_{\mathrm{m,L}}}{\partial t} - V_{\mathrm{m,L}} = \lambda_{0_{\mathrm{J}}}^2 \frac{\rho_{\mathrm{e}} b}{2d}\frac{\partial J_{\mathrm{e},z}}{\partial z}$
Transverse	$\tau_{\mathrm{T,J}}\frac{d\check{V}_{\mathrm{m,T}}^{\mathrm{Max}}}{dt} + \check{V}_{\mathrm{m,T}}^{\mathrm{Max}} = -\frac{R_{\mathrm{m}} R_{\mathrm{e,J}}(1)\check{J}_{\mathrm{e,T}}}{(R_{\mathrm{m}} + R_{\mathrm{i},J}(1) + R_{\mathrm{e},J}(1))}$	$\tau_{\mathrm{T,J}}\frac{dV_{\mathrm{m,T}}^{\mathrm{Max}}}{dt} + V_{\mathrm{m,T}}^{\mathrm{Max}} = -\frac{R_{\mathrm{m}} R_{\mathrm{e,J}}(1) J_{\mathrm{e,T}}}{(R_{\mathrm{m}} + R_{\mathrm{i},J}(1) + R_{\mathrm{e},J}(1))}$

Appendix D. Equivalence of Bidomain and Volume Conductor Formalisms

Here it is shown that the bidomain and volume conductor formalisms are mathematically equivalent in the sense that the quantities values obtained for V_e, V_i, $V_\mathrm{m,L}$ and $V_\mathrm{m,T}$ are independent of which formalism is used. This is demonstrated by showing that the problem of determining these four quantities using the bidomain formalism can be transformed into the problem of solving the equations for these four quantities in the volume conductor formalism.

Appendix D.1. Fibre Bundle

The proof is carried out in the Fourier (k,ω)-coordinates. Equations (24a) and (24b) may be written in these coordinates as

$$\sigma_\mathrm{i,L}^\mathrm{bd} k_z^2 \hat{\hat{V}}_\mathrm{i}^\mathrm{bd} + \frac{\beta}{Z_\mathrm{m}(\omega)} \hat{\hat{V}}_\mathrm{m}^\mathrm{bd} = 0, \tag{D.1}$$

$$-\sigma_\mathrm{e,T}^\mathrm{bd} \boldsymbol{\nabla}_\mathrm{T}^2 \hat{\hat{V}}_\mathrm{e}^\mathrm{bd} + \sigma_\mathrm{e,L}^\mathrm{bd} k_z^2 \hat{\hat{V}}_\mathrm{e}^\mathrm{bd} - \frac{\beta}{Z_\mathrm{m}(\omega)} \hat{\hat{V}}_\mathrm{m}^\mathrm{bd} = 0. \tag{D.2}$$

The notation $\boldsymbol{\nabla}_\mathrm{T}$ denotes the (x,y) part of the $\boldsymbol{\nabla}$ operator.

$\hat{\hat{V}}_\mathrm{m}$ and subsequently $\hat{\hat{V}}_\mathrm{i}$ can be eliminated from Equation (D.2) by substitution with Equation (D.1) and using $\hat{\hat{V}}_\mathrm{m} = \hat{\hat{V}}_\mathrm{i} - \hat{\hat{V}}_\mathrm{e}$ to give an equation involving only the voltage variable $\hat{\hat{V}}_\mathrm{e}$

$$\sigma_\mathrm{e,T}^\mathrm{bd} \boldsymbol{\nabla}_\mathrm{T}^2 \hat{\hat{V}}_\mathrm{e}^\mathrm{bd} - (\sigma_\mathrm{e,L}^\mathrm{bd} + \sigma_\mathrm{i,L}^\mathrm{bd}) \left(\frac{1 + \frac{Z_\mathrm{m}\sigma_\mathrm{e,L}^\mathrm{bd}\sigma_\mathrm{i,L}^\mathrm{bd}}{\beta\sigma_\mathrm{e,L}^\mathrm{bd} + \sigma_\mathrm{i,L}^\mathrm{bd}} k_z^2}{1 + \frac{Z_\mathrm{m}\sigma_\mathrm{i,L}^\mathrm{bd}}{\beta} k_z^2} \right) k_z^2 \hat{\hat{V}}_\mathrm{e} = 0. \tag{D.3}$$

The following expressions in the above equation may be simplified as follows

$$\sigma_\mathrm{e,L}^\mathrm{bd} + \sigma_\mathrm{i,L}^\mathrm{bd} = \frac{r_\mathrm{e} + r_\mathrm{i}}{\pi b^2 r_\mathrm{e} r_\mathrm{i}} \approx \frac{1}{\rho_\mathrm{i}}, \quad r_\mathrm{i} \ll r_\mathrm{e}, \tag{D.4}$$

$$\frac{Z_\mathrm{m}\sigma_\mathrm{e,L}^\mathrm{bd}\sigma_\mathrm{i,L}^\mathrm{bd}}{\beta\sigma_\mathrm{e,L}^\mathrm{bd} + \sigma_\mathrm{i,L}^\mathrm{bd}} = \lambda_\mathrm{J}^2(\omega), \tag{D.5}$$

$$\frac{Z_\mathrm{m}\sigma_\mathrm{i,L}^\mathrm{bd}}{\beta} = \lambda_\mathrm{V}^2(\omega). \tag{D.6}$$

Substituting these into Equation (D.3) and noting $\sigma_\mathrm{e,T}^\mathrm{bd} = \sigma_\mathrm{e,T}^\mathrm{vc}$ leads to

$$\sigma_\mathrm{e,T}^\mathrm{bd} \boldsymbol{\nabla}_\mathrm{T}^2 \hat{\hat{V}}_\mathrm{e}^\mathrm{bd} - \frac{r_\mathrm{e} + r_\mathrm{i}}{\pi b^2 r_\mathrm{e} r_\mathrm{i}} \left(\frac{1 + \lambda_\mathrm{J}^2 k_z^2}{1 + \lambda_\mathrm{V}^2 k_z^2} \right) k_z^2 \hat{\hat{V}}_\mathrm{e} = 0, \tag{D.7}$$

which is the fundamental equation determining V_e for the volume conductor formalism in (k_z,ω) coordinates.

The equation for $\hat{\hat{V}}_\mathrm{m,L}^\mathrm{bd}$ can be derived solving for $\hat{\hat{V}}_\mathrm{m,L}^\mathrm{bd}$ in Equation (D.2) and then

eliminating the term containing $\boldsymbol{\nabla}_{\mathrm{T}}^2$ using Equation (D.7) to give

$$\begin{aligned}\hat{\hat{V}}_{\mathrm{m,L}}^{\mathrm{bd}} &= -\left[\frac{\beta(r_{\mathrm{e}}+r_{\mathrm{i}})}{\pi b^2 Z_{\mathrm{m}} r_{\mathrm{e}} r_{\mathrm{i}}}\left(\frac{1+\lambda_{\mathrm{J}}^2 k_z^2}{1+\lambda_{\mathrm{V}}^2 k_z^2}\right)+\frac{\beta}{\pi b^2 Z_{\mathrm{m}} r_{\mathrm{e}}}\right] k_z^2 \hat{\hat{V}}_{\mathrm{e}}^{\mathrm{bd}} \\ &= -\frac{z_{\mathrm{m}}(\lambda_{\mathrm{J}}^2-\lambda_{\mathrm{V}}^2)}{r_{\mathrm{e}}\lambda_{\mathrm{J}}^2(1+k_z^2\lambda_{\mathrm{V}}^2)} k_z^2 \hat{\hat{V}}_{\mathrm{e}}^{\mathrm{bd}} \\ &= -\frac{k_z^2\lambda_{\mathrm{V}}^2}{1+k_z^2\lambda_{\mathrm{V}}^2}\hat{\hat{V}}_{\mathrm{e}}^{\mathrm{bd}}. \end{aligned} \tag{D.8}$$

This is the cable equation for voltage boundary conditions that applies for the volume conductor formalism. It relates $\hat{\hat{V}}_{\mathrm{m,L}}^{\mathrm{bd}}$ to $\hat{\hat{V}}_{\mathrm{e}}^{\mathrm{bd}}$. As we have already shown that $\hat{\hat{V}}_{\mathrm{e}}^{\mathrm{bd}}$ is determined by the same equation for both formalisms, this now shows that $\hat{\hat{V}}_{\mathrm{m,L}}^{\mathrm{bd}}$ is too. In obtaining the equation above we made use of the identities $Z_{\mathrm{m}} = 2\pi b z_{\mathrm{m}}$ (relating the unit area membrane impedance to the unit length membrane impedance), $\lambda_{\mathrm{V}}^2 = z_{\mathrm{m}}/r_{\mathrm{i}}$ and $\lambda_{\mathrm{J}}^2 = z_{\mathrm{m}}/(r_{\mathrm{e}}+r_{\mathrm{i}})$.

Finally, for both formalisms, $\hat{\hat{V}}_{\mathrm{i}}^{\mathrm{bd}}$ may be obtained from $\hat{\hat{V}}_{\mathrm{e}}^{\mathrm{bd}}$ and $\hat{\hat{V}}_{\mathrm{m,L}}^{\mathrm{bd}}$ via $\hat{\hat{V}}_{\mathrm{i}}^{\mathrm{bd}} = \hat{\hat{V}}_{\mathrm{e}}^{\mathrm{bd}} + \hat{\hat{V}}_{\mathrm{m,L}}^{\mathrm{bd}}$.

Appendix D.2. General Case

The proof is analogous to the fibre bundle case, except that it is carried out in $(\mathbf{k},\omega)$ Fourier domain with a three dimensional spatial transform instead of just a one dimensional transform.

Following similar steps one obtains and equation analogous to Equation (D.3)

$$\sum_{h=1}^{H}\alpha_h \mathbf{k}^T\left(\frac{\hat{\hat{\boldsymbol{\sigma}}}_{\mathrm{e},h}^{\mathrm{bd}}+\hat{\hat{\boldsymbol{\sigma}}}_{\mathrm{i},h}^{\mathrm{bd}}+\beta_h^{-1}Z_{\mathrm{m}}(\mathbf{k}^T\hat{\hat{\boldsymbol{\sigma}}}_{\mathrm{i},h}^{\mathrm{bd}}\mathbf{k})\hat{\hat{\boldsymbol{\sigma}}}_{\mathrm{i},h}^{\mathrm{bd}}}{1+\mathbf{k}^T\hat{\hat{\boldsymbol{\sigma}}}_{\mathrm{i},h}^{\mathrm{bd}}\mathbf{k}}\right)\mathbf{k}\hat{\hat{V}}_{\mathrm{e}} = 0. \tag{D.9}$$

From Equations (30g) and (D.6) we find that

$$\mathbf{k}^T\hat{\hat{\boldsymbol{\sigma}}}_{\mathrm{i},h}^{\mathrm{bd}}\mathbf{k}\beta_h^{-1}Z_{\mathrm{m}} = \lambda_{\mathrm{V}}^2(\omega)(\mathbf{k}\cdot u). \tag{D.10}$$

Substituting this into Equation (D.9) as well as Equations (30g), (30h) one can rearrange to get

$$\sum_{h=1}^{H}\alpha_h\mathbf{k}^T\left[\hat{\hat{\sigma}}_{\mathrm{e,T},h}^{\mathrm{bd}}\mathbf{I}+\left(\frac{(\hat{\hat{\sigma}}_{\mathrm{i,L},h}^{\mathrm{bd}}\hat{\hat{\sigma}}_{\mathrm{e,L},h}^{\mathrm{bd}})+\lambda_{\mathrm{V}}^2(\omega)(\mathbf{k}\cdot\mathbf{u})^2\hat{\hat{\sigma}}_{\mathrm{e,L},h}^{\mathrm{bd}}}{1+\lambda_{\mathrm{V}}^2(\omega)(\mathbf{k}\cdot\mathbf{u})^2}-\hat{\hat{\sigma}}_{\mathrm{e,T},h}^{\mathrm{bd}}\right)\mathbf{u}\mathbf{u}^T\right]\mathbf{k}\hat{\hat{V}}_{\mathrm{e}} = 0. \tag{D.11}$$

Using the identities (D.4)-(D.6) together with $\hat{\hat{\sigma}}_{\mathrm{e,T},h}^{\mathrm{bd}} = \hat{\hat{\sigma}}_{\mathrm{e,T},h}^{\mathrm{vc}}$ then gives fundamental equation governing V_{e} in the generalised volume conductor model:

$$\sum_{h=1}^{H}\alpha_h\mathbf{k}^T\left[\hat{\hat{\sigma}}_{\mathrm{e,T},h}^{\mathrm{vc}}\mathbf{I}+\left(\frac{\rho_{\mathrm{i}}^{-1}(1+\lambda_{\mathrm{J}}^2(\omega)(\mathbf{k}\cdot\mathbf{u})^2)}{1+\lambda_{\mathrm{V}}^2(\omega)(\mathbf{k}\cdot\mathbf{u})^2}-\hat{\hat{\sigma}}_{\mathrm{e,T},h}^{\mathrm{vc}}\right)\mathbf{u}\mathbf{u}^T\right]\mathbf{k}\hat{\hat{V}}_{\mathrm{e}} = 0. \tag{D.12}$$

References

[1] H. Kasi, W. Hasenkamp, G. Cosendai, A. Bertsch, and P. Renaud. Simulation of epiretinal prostheses-evaluation of geometrical factors affecting stimulation thresholds. *Journal of Neuroengineering and Rehabilitation*, 8:44, 2011.

[2] J. Rizzo, J. Tombran-Tink, and C.J. Barnstable. *Visual Prosthesis and Ophthalmic Devices: New Hope in Sight*. Ophthalmology Research. Humana, 2007.

[3] J.C. Martins. *Bioelectronic Vision: Retina Models, Evaluation Metrics and System Design*. BE&BME Vol.3, World Scientific, 2009.

[4] G. Clark. *Cochlear Implants: Fundamentals and Applications*. Springer-Verlag, 2003.

[5] P.G. Patil and D.A. Turner. The development of brain-machine interface neuroprosthetic devices. *Neurotherapeutics*, 5(1):137 – 146, 2008.

[6] J.K. Niparko. *Cochlear Implants: Principles & Practices*. Williams & Wilkins, 2nd edition, 2009.

[7] D. Andreu, D. Guiraud, and G. Souquet. A distributed architecture for activating the peripheral nervous system. *Journal of Neural Engineering*, 6(2):026001, 2009.

[8] S. Micera, J. Carpaneto, and S. Raspopovic. Control of hand prostheses using peripheral information. *Biomedical Engineering, IEEE Reviews in*, 3:48 –68, 2010.

[9] G.H. Baltuch and M.B. Stern. *Deep Brain Stimulation for Parkinson'S Disease*. Informa Healthcare, 2007.

[10] E.B. Montgomery. *Deep Brain Stimulation Programming: Principles and Practice*. Oxford University Press, 2010.

[11] D.R. McNeal. Analysis of a model for excitation of myelinated nerve. *IEEE Transactions on Biomedical Engineering*, 23(4):329 – 337, 1976.

[12] F. Rattay. Analysis of models for extracellular fiber stimulation. *IEEE Transaction on Biomedical Engineering*, 36(7):676–682, 1989.

[13] N. Trayanova, C.S. Henriquez, and R. Plonsey. Extracellular potentials and currents of a single active fiber in a restricted volume conductor. *Annals of Biomedical Engineering*, 18(3):219 – 238, 1990.

[14] D.A. Stewart, Jr., T.R. Gowrishankar, K.C. Smith, and J.C. Weaver. Cylindrical cell membranes in uniform applied electric fields: Validation of a transport lattice method. *IEEE Transactions on Biomedical Engineering*, 52(10):1643 – 1653, 2005.

[15] W. Ying and C.S. Henriquez. Hybrid finite element method for describing the electrical response of biological cells to applied fields. *IEEE Transactions on Biomedical Engineering*, 54(4):611 – 620, 2007.

[16] G. Pucihar, D. Miklavcic, and T. Kotnik. A time-dependent numerical model of transmembrane voltage inducement and electroporation of irregularly shaped cells. *IEEE Transactions on Biomedical Engineering*, 56(5):1491–1501, 2009.

[17] D. Boinagrov, J. Loudin, and D. Palanker. Strength-Duration Relationship for Extracellular Neural Stimulation: Numerical and Analytical Models. *Journal of Neurophysiology*, 104(4):2236–2248, 2010.

[18] S. Joucla, L. Rousseau, and B. Yvert. Focalizing electrical neural stimulation with penetrating microelectrode arrays: A modeling study. *Journal of Neuroscience Methods*, 209(1):250 – 254, 2012.

[19] S. Joucla, P. Branchereau, D. Cattaert, and B. Yvert. Extracellular neural microstimulation may activate much larger regions than expected by simulations: A combined experimental and modeling study. *PLoS ONE*, 7(8):e41324, 2012.

[20] A. Van Harreveld and S.K. Malhotra. Extracellular space in the cerebral cortex of the mouse. *Journal of Anatomy*, 101:197 – 207, 1967.

[21] A. Van Harreveld and F.I. Khattab. Changes in extracellular space of the mouse cerebral cortex during hydroxyadipaldehyde fixation and osmium tetroxide post-fixation. *Journal of Cell Science*, 4(2):437 – 453, 1969.

[22] A. Lehmenkühler, E. Sykova, J. Svoboda, K. Zilles, and C. Nicholson. Extracellular space parameters in the rat neocortex and subcortical white matter during postnatal development determined by diffusion analysis. *Neuroscience*, 55(2):339 – 351, 1993.

[23] E. Sykova and C. Nicholson. Diffusion in brain extracellular space. *Physiological Reviews*, 88(4):1277 – 1340, 2008.

[24] Y. Mishchenko, T. Hu, J.Spacek, J. Mendenhall, K.M. Harris, and D.B. Chklovskii. Ultrastructural analysis of hippocampal neuropil from the connectomics perspective. *Neuron*, 67(6):1009–1020, 2010.

[25] H. Meffin, B. Tahayori, D.B. Grayden, and A.N. Burkitt. Modeling extracellular electrical stimulation: I. Derivation and interpretation of neurite equations. *Journal of Neural Engineering*, 9:065005, 2012.

[26] Jaakko Malmivuo and Robert Plonsey. *Bioelectromagnetism : Principles and Applications of Bioelectric and Biomagnetic Fields*. Oxford University Press, USA, 1995.

[27] B. Tahayori, H. Meffin, S. Dokos, A.N. Burkitt, and D.B. Grayden. Modeling extracellular electrical stimulation: II. Computational validation and numerical results. *Journal of Neural Engineering*, 9:065006, 2012.

[28] S. Joucla and B. Yvert. Modeling extracellular electrical neural stimulation: From basic understanding to MEA-based applications. *Journal of Physiology-Paris*, 106:146 – 158, 2012.

[29] H. Meffin, B. Tahayori, D.B. Grayden, and A.N. Burkitt. Internal inconsistencies in models of electrical stimulation in neural tissue. In *Engineering in Medicine and Biology Society (EMBC), 2013 Annual International Conference of the IEEE*, pages 5946–5949, 2013.

[30] M. Pavlin, N. Pavselj, and D. Miklavcic. Dependence of induced transmembrane potential on cell density, arrangement, and cell position inside a cell system. *IEEE Transactions on Bio-Medical Engineering*, 49(6):605 – 612, 2002.

[31] N. Pourtaheri, W. Ying, J.M. Kim, and C.S. Henriquez. Thresholds for transverse stimulation: fiber bundles in a uniform field. *IEEE Transactions on Neural Systems and Rehabilitation Engineering*, 17(5):478 – 486, 2009.

[32] B.J. Roth and J.P. Wikswo. Electrical stimulation of cardiac tissue: A bidomain model with active membrane properties. *IEEE Transactions on Biomedical Engineering*, 41(3):232–240, 1994.

[33] S. Dokos, G.J. Suaning, and N.H. Lovell. A bidomain model of epiretinal stimulation. *IEEE Transactions on Neural Systems and Rehabilitation Engineering*, 13(2):137–146, 2005.

[34] S. Joucla, A. Gliere, and B. Yvert. Current approaches to model extracellular electrical neural microstimulation. *Frontiers in Computational Neuroscience*, 8(13), 2014.

[35] L. Borcea. Electrical impedance tomography. *Inverse Problems*, 18(6):R99–R136, 2002.

[36] H. Meffin and T. Kameneva. The electrotonic length constant: A theoretical estimate for neuroprosthetic electrical stimulation. *Biomedical Signal Processing and Control*, 6(2):105 – 111, 2011.

[37] D.K. Cheng. *Field and Wave Electromagnetics*. Addison Wesley, 2nd edition, 1989.

[38] R. Plonsey and R.C. Barr. *Bioelectricity: A Quantitative Approach*. Springer, 3rd edition, 2007.

[39] F. Rattay. Analysis of models for external stimulation of axons. *IEEE Transactions on Bio-Medical Engineering*, 33(10):974 – 977, 1986.

[40] M. Abramian, N.H. Novell, J.W. Morely, G.J. Suaning, and S. Dokos. Activation of retinal ganglion cells following epiretinal electrical stimulation with hexagonally arranged bipolar electrodes. *Journal of Neural Engineering*, 8:035004, 2011.

[41] C.R. Butson and C.C. McIntyre. Tissue and electrode capacitance reduce neural activation volumes during deep brain stimulation. *Clinical Neurophysiology*, 116(10):2490–2500, 2005.

[42] B. Tahayori, H. Meffin, E.N. Sergeev, Iven M.Y. Mareels, A.N. Burkitt, and D.B. Grayden. Modeling extracellular electrical stimulation: IV. Effect of the cellular composition of neural tissue on its spatio-temporal filtering properties. *Journal of Neural Engineering*, 2014.

[43] S.I. Fried, A.C.W. Lasker, n.J. Desai, D.K. Eddington, and JF. Rizzo. Axonal sodium-channel bands shape the response to electric stimulation in retinal ganglion cells. *Journal*

of Neurophysiology, 101(4):1972–1987, 2009.

[44] M. Pavlin and D. Miklavcic. The effective conductivity and the induced transmembrane potential in dense cell system exposed to dc and ac electric fields. *IEEE Transactions on Plasma Science*, 37(1):99–106, 2009.

[45] J.B. Ranck, Jr. Analysis of specific impedance of rabbit cerebral cortex. *Experimental Neurology*, 7(2):153–174, 1963.

[46] B. J. Roth. Bidomain model. *Scholarpedia*, 3(4):6221, 2008.

[47] K.W. Altman and R. Plonsey. Analysis of excitable cell activation: relative effects of external electrical stimuli. *Medical & Biological Engineering & Computing*, 28(6):574 – 580, 1990.

[48] M. Solomonow. Comments, with reply, on "Point source nerve bundle stimulation: effects of fiber diameter and depth on simulated excitation" by K.W. Altman and R. Plonsey. *IEEE Transactions on Biomedical Engineering*, 38(4):390, 1991.

[49] A. Destexhe, D. Contreras, and M. Steriade. Spatiotemporal analysis of local field potentials and unit discharges in cat cerebral cortex during natural wake and sleep states. *The Journal of Neuroscience*, 19(11):4595–4608, 1999.

[50] C. Bédard, H. Kröger, and A. Destexhe. Modeling extracellular field potentials and the frequency-filtering properties of extracellular space. *Biophysical Journal*, 86(3):1829 – 1842, 2004.

[51] C. Gabriel, S. Gabriel, and E. Corthout. The dielectric properties of biological tissues: I. Literature survey. *Physics in Medicine and Biology*, 41(11):2231, 1996.